The entropy solutions for the Lighthill-Whitham-Richards traffic flow model with a discontinuous flow-density relationship

Yadong Lu[1], S.C. Wong[2], Mengping Zhang[3], Chi-Wang Shu[4]

Abstract

In this paper we explicitly construct the entropy solutions for the Lighthill-Whitham-Richards (LWR) traffic flow model with a flow-density relationship which is piecewise quadratic, concave, but not continuous at the junction points where two quadratic polynomials meet, and with piecewise linear initial condition and piecewise constant boundary conditions. The existence and uniqueness of entropy solutions for such conservation laws with discontinuous fluxes are not known mathematically. We have used the approach of explicitly constructing the entropy solutions to a sequence of approximate problems in which the flow-density relationship is continuous but tends to the discontinuous flux when a small parameter in this sequence tends to zero. The limit of the entropy solutions for this sequence is explicitly constructed and is considered to be the entropy solution associated with the discontinuous flux. We apply this entropy solution construction procedure to solve three representative traffic flow cases, compare them with numerical solutions obtained by a high order weighted essentially non-oscillatory (WENO) scheme, and discuss the results from traffic flow perspectives.

Key Words: LWR model; traffic flow; discontinuous flow-density relationship; entropy solution; WENO scheme

[1]Department of Mathematics, University of Science and Technology of China, Hefei, Anhui 230026, China. E-mail: luyd@mail.ustc.edu.cn

[2]Department of Civil Engineering, The University of Hong Kong, Hong Kong, China. E-mail: hhecwsc@hkucc.hku.hk

[3]Department of Mathematics, University of Science and Technology of China, Hefei, Anhui 230026, China. E-mail: mpzhang@ustc.edu.cn

[4]Division of Applied Mathematics, Brown University, Providence, RI 02912, USA. E-mail: shu@dam.brown.edu

Report Documentation Page

Form Approved
OMB No. 0704-0188

1. REPORT DATE	2. REPORT TYPE	3. DATES COVERED
2007		**00-00-2007 to 00-00-2007**

4. TITLE AND SUBTITLE	5a. CONTRACT NUMBER
The entropy solutions for the Lighthill-Whitham-Richards traffic flow model with a discontinuous flow-density relationship	5b. GRANT NUMBER
	5c. PROGRAM ELEMENT NUMBER
6. AUTHOR(S)	5d. PROJECT NUMBER
	5e. TASK NUMBER
	5f. WORK UNIT NUMBER
7. PERFORMING ORGANIZATION NAME(S) AND ADDRESS(ES) **Brown University,Division of Applied Mathematics,Providence,RI,02912**	8. PERFORMING ORGANIZATION REPORT NUMBER
9. SPONSORING/MONITORING AGENCY NAME(S) AND ADDRESS(ES)	10. SPONSOR/MONITOR'S ACRONYM(S)
	11. SPONSOR/MONITOR'S REPORT NUMBER(S)

12. DISTRIBUTION/AVAILABILITY STATEMENT
Approved for public release; distribution unlimited

13. SUPPLEMENTARY NOTES
The original document contains color images.

14. ABSTRACT

15. SUBJECT TERMS

16. SECURITY CLASSIFICATION OF:			17. LIMITATION OF ABSTRACT	18. NUMBER OF PAGES	19a. NAME OF RESPONSIBLE PERSON
a. REPORT **unclassified**	b. ABSTRACT **unclassified**	c. THIS PAGE **unclassified**		**42**	

1 Introduction

Lighthill and Whitham (1955) and Richards (1956) independently proposed a macroscopic model of traffic flow to describe the dynamic characteristics of traffic on a homogeneous and unidirectional highway, which is now known as the LWR model in the literature of traffic flow theory. Although a substantial amount of work has been conducted to improve the modeling approach of traffic flows in many directions, the LWR model is still widely used for the modeling of traffic flow, because of its simplicity and good explanatory power to understand the qualitative behavior of road traffic. The results that are obtained from the LWR model are generally adequate for many applications such as traffic management and control problems.

The LWR model is formulated as a scalar hyperbolic conservation law and is often solved by finite difference methods (Daganzo, 1995; LeVeque, 1992; Lebacque, 1996; Michalopoulos et al., 1984; Wong and Wong, 2002a; Zhang et al., 2003). The main difficulty in designing efficient and high order finite difference methods for the LWR model or in general for hyperbolic conservation laws is the inherent presence of discontinuities (shocks) in the solution (Lebacque, 1996). Moreover, discontinuous weak solutions are not unique for hyperbolic conservation laws and entropy conditions must be satisfied to obtain physically valid solution that is consistent with human behavior (such as the driver's ride impulse) (Ansorge, 1990; Velan and Florian, 2002). Recently, the analytical solution for specific classes of LWR model was derived, which assumed that the flow-density relationship is governed by a quadratic function throughout the density regime (Wong and Wong, 2002b), and then extended to the case of a piecewise quadratic function (Lu et al., 2006). Their constructed entropy solutions are exact if the initial condition is piecewise linear and the boundary condition is piecewise constant. The fundamental diagrams in their works are continuous.

However, when traffic flow data are plotted on the fundamental diagram, the uncongested and congested regimes may be separated by gaps or discontinuities as shown in Figure 1. Edie (1961) was among the first to point out that traffic behaved differently at different

density regimes, and introduced the idea of a two-regime model leading to a discontinuous fundamental diagram. The discontinuous fundamental diagrams have also been observed from empirical works (e.g., Ceder, 1976; Ceder and May, 1976; Drake et al., 1967; May and Keller, 1967). In particular, Koshi et al. (1983) suggested a "reverse lambda" shape to describe the characteristics of the data plotted on the discontinuous fundamental diagrams. Further evidence of the discontinuous fundamental diagram was revealed by a series of papers by Hall (1987), Hall and Gunter (1986) and Hall et al. (1986). In addition, Bank (1991a,b) described this discontinuous fundamental diagram as a two-capacity phenomenon, with one capacity corresponding to the tip of the left leg of the reverse lambda, and the other capacity belonging to the tip of the right leg of the reverse lambda with a capacity drop from the former tip. More recently, Cassidy (1998) and Cassidy and Bertini (1999) also confirmed the capacity drop on highways. When such discontinuous fundamental diagram is embedded into the LWR model, it is to our best knowledge that there is still no mathematical theory on the existence and uniqueness of the entropy solutions for the resultant traffic model.

In this paper we assume that the flow-density relationship $q(\rho)$ is concave and is represented by a piecewise quadratic function, with any two adjacent pieces joining discontinuously at a critical density ρ_0. Such discontinuous fundamental diagrams were developed in Drake et al. (1967) by fitting with observed data. Our procedure to construct the physically relevant solutions for such conservation laws with discontinuous fluxes is as follows. We first explicitly construct the entropy solutions to a sequence of approximate problems in which the flow-density relationship $q(\rho)$ is continuous but tends to the discontinuous flux when a small parameter in this sequence tends to zero. We then explicitly construct the limit of the entropy solutions for this sequence and consider this limit solution as the the entropy solution associated with the discontinuous flux. In order to verify the physical relevancy of such entropy solutions, we apply our results to a few typical traffic flow examples and comment on the implication of the solutions.

The organization of the paper is as follows. In Section 2 we obtain the explicit formulas

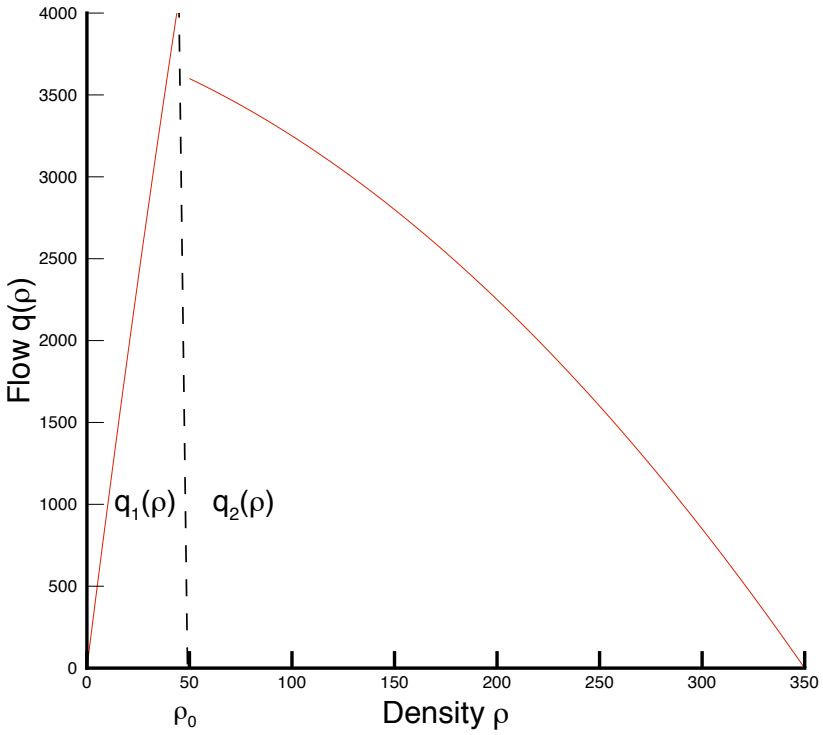

Figure 1: A typical flow with two different concave quadratic functions joining discontinuously at a critical density ρ_0 with decreasing derivative at ρ_0.

for the entropy solutions to Riemann problems with discontinuous flow-density relationship, in a limit process involving a sequence of approximate problems in which the flow-density relationship $q(\rho)$ is continuous but tends to the discontinuous flux when a small parameter in this sequence tends to zero. In Section 3 we obtain the explicit formulas for the entropy solutions with discontinuous flow-density relationship and with piecewise linear initial condition and piecewise constant boundary conditions. In Section 4 we provide numerical examples in traffic flows to demonstrate the explicit solutions obtained in Sections 2 and 3. We also compare these explicit solutions with numerical solutions obtained by using the high order weighted essentially non-oscillatory (WENO) schemes (Jiang and Shu, 1996; Zhang et al., 2003). Concluding remarks are given in Section 5.

2 A sequence of approximate problems with continuous fluxes: Riemann problems

The governing equation for the LWR model is the following scalar hyperbolic conservation law

$$\rho_t + q(\rho)_x = 0 \tag{1}$$

with suitable initial and boundary conditions. Here $\rho \in (0, \rho_{\max})$ is the density, $\rho_{\max}$ is the maximum (jam) density, and $q(\rho)$ is the traffic flow on a homogeneous highway, which is assumed to be a function of the density ρ only in the LWR model. More specifically, the flow q, the density ρ and the equilibrium speed u are related by

$$q(\rho) = u(\rho)\,\rho. \tag{2}$$

In this paper, the flow $q(\rho)$ is considered to be piecewise quadratic and locally concave in each piece. Without loss of generality, we will concentrate our discussion on the situation where the flow q is defined by two different quadratic functions in different regimes

$$q(\rho) = \begin{cases} q_1(\rho), & 0 \le \rho \le \rho_0 \\ q_2(\rho), & \rho_0 < \rho \le \rho_{\max} \end{cases} \tag{3}$$

where

$$\text{Flux I: } q_1(\rho) = d_0 + d_1\,\rho + d_2\,\rho^2; \qquad \text{Flux II: } q_2(\rho) = e_0 + e_1\,\rho + e_2\,\rho^2 \tag{4}$$

are two different quadratic functions, which are discontinuous at the junction $q_1(\rho_0) > q_2(\rho_0)$, concave in each piece $q_1''(\rho) < 0$ and $q_2''(\rho) < 0$, and concave also at the junction $q_1'(\rho_0) \ge q_2'(\rho_0)$.

A typical flow in this setup is given in Figure 1. The general situation of the flow q with more than two pieces of quadratic functions can be considered with the same recipe to each neighboring pairs of quadratic flow functions.

Since it is not known mathematically how to study the existence and uniqueness of entropy solutions for the scalar conservation law (1) with a discontinuous flux function $q(\rho)$,

we first consider the following sequence of conservation laws with continuous fluxes

$$\rho_t + q^\varepsilon(\rho)_x = 0 \tag{5}$$

where

$$q^\varepsilon(\rho) = \begin{cases} q_1(\rho) = d_2\rho^2 + d_1\rho + d_0, & 0 \le \rho \le \rho_0 \\ q^\varepsilon_{mid}(\rho) = -\frac{q_1(\rho_0) - q_2^\varepsilon(\rho_0+\varepsilon)}{\varepsilon}(\rho - \rho_0) + q_1(\rho_0), & \rho_0 < \rho \le \rho_0 + \varepsilon \\ q_2^\varepsilon(\rho) = e_2\rho^2 + (e_1 - 2\varepsilon e_2)\rho + e_0 + e_2\varepsilon^2 - e_1\varepsilon, & \rho_0 + \varepsilon < \rho \le \rho_{\max} \end{cases} \tag{6}$$

with a simple Riemann type initial condition

$$\rho(x,0) = \begin{cases} \rho_l, & x \le 0 \\ \rho_r, & x > 0 \end{cases} . \tag{7}$$

Notice that the narrow ε region connecting the two pieces of the discontinuous fluxes is located to the right of the discontinuity point ρ_0. We could of course also construct the sequence with the narrow ε region located to the left of the discontinuity point ρ_0, or centrally around ρ_0.

We remark here the technical difficulty in dealing with the conservation law (1) with the flux (6): the flux is continuous for $\varepsilon > 0$, but it is not globally concave. Therefore, we cannot use our results in (Lu et al., 2006) directly. It is not possible to connect the two discontinuous pieces of the flux in a continuous and globally concave fashion.

We are interested only in the situations that $\rho_l \le \rho_0 \le \rho_r$ or $\rho_l \ge \rho_0 \ge \rho_r$, with the equality holding at most once in each situation. Otherwise, the Riemann problem would involve only one of the two quadratic fluxes in (4) and its solution would be routine.

Even though the flux $q^\varepsilon(\rho)$ is not globally concave, it is continuous for $\varepsilon > 0$. Therefore, we can construct the solution to the Riemann problem using standard techniques, see, e.g. (LeVeque, 1992), via convex or concave hulls from the graph of the flux $q^\epsilon(\rho)$.

2.1 Shock: $\rho_l < \rho_r$

If $\rho_l < \rho_r$, and without loss of generality assume $\rho_l \le \rho_0 < \rho_0 + \varepsilon \le \rho_r$, then we construct the convex hull of the set $\{(\rho, y) : \rho_l \le \rho \le \rho_r \ \textit{and} \ y \ge q^\varepsilon(\rho)\}$. Recall that the convex hull is the smallest convex set containing the original set. An illustration of the convex hull is

shown in Figures 2 and 3 (the shaded region). We can then obtain the entropy solution of the Riemann problem with the flux $q^\varepsilon(\rho)$ as follows, where $\xi = x/t$:

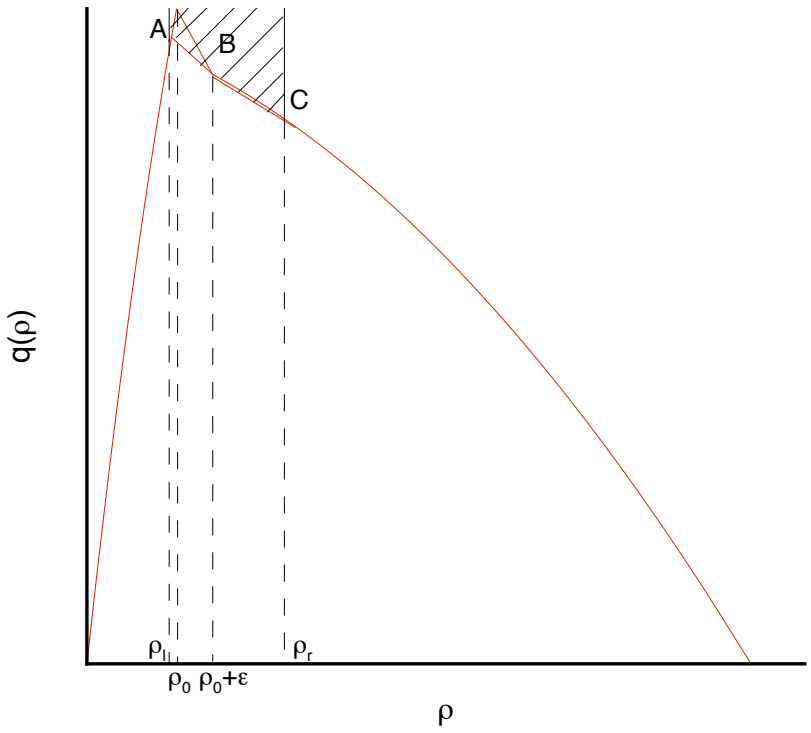

Figure 2: The convex hull of $\{(\rho, y) : \rho_l \le \rho \le \rho_r \ \ and \ \ y \ge q^\varepsilon(\rho)\}$ for $k_{AB} < k_{BC}$.

Let k_{AB} and k_{BC} be the slope of AB and the slope of BC, respectively, where

$$k_{AB} = \frac{q_2^\varepsilon(\rho_0 + \varepsilon) - q_1(\rho_l)}{\rho_0 + \varepsilon - \rho_l}, \qquad k_{BC} = \frac{q_2^\varepsilon(\rho_r) - q_2^\varepsilon(\rho_0 + \varepsilon)}{\rho_r - (\rho_0 + \varepsilon)}$$

- If

$$k_{AB} < k_{BC}, \tag{8}$$

then the solution is (see Figure 2)

$$\rho(x,t) = \begin{cases} \rho_l, & \xi \le k_{AB} \\ \rho_0 + \varepsilon, & k_{AB} < \xi < k_{BC} \\ \rho_r, & \xi \ge k_{BC} \end{cases} \tag{9}$$

- If

$$k_{AB} \ge k_{BC}, \tag{10}$$

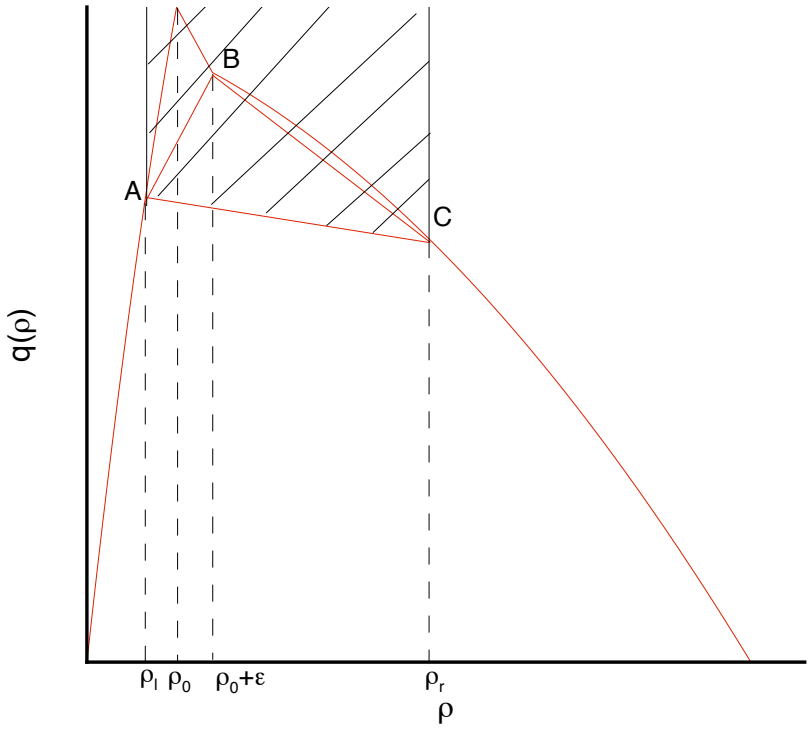

Figure 3: The convex hull of $\{(\rho, y) : \rho_l \le \rho \le \rho_r \ \ and \ \ y \ge q^\varepsilon(\rho)\}$ for $k_{AB} \ge k_{BC}$.

then the solution is (see Figure 3)

$$\rho(x,t) = \begin{cases} \rho_l, & \xi \le \frac{q_2^\varepsilon(\rho_r) - q_1(\rho_l)}{\rho_r - \rho_l} \\ \rho_r, & \xi > \frac{q_2^\varepsilon(\rho_r) - q_1(\rho_l)}{\rho_r - \rho_l} \end{cases} \tag{11}$$

Therefore, taking the limit $\varepsilon \to 0^+$, we have the following explicit solutions to the Riemann problem with the discontinuous flux (3) :

- If

$$\frac{q_2(\rho_0) - q_1(\rho_l)}{\rho_0 - \rho_l} < \frac{q_2(\rho_r) - q_2(\rho_0)}{\rho_r - \rho_0} \tag{12}$$

then

$$\rho(x,t) = \begin{cases} \rho_l, & \xi \le \frac{q_2(\rho_0) - q_1(\rho_l)}{\rho_0 - \rho_l} \\ \rho_0, & \frac{q_2(\rho_0) - q_1(\rho_l)}{\rho_0 - \rho_l} < \xi < \frac{q_2(\rho_r) - q_2(\rho_0)}{\rho_r - \rho_0} \\ \rho_r, & \xi \ge \frac{q_2(\rho_r) - q_2(\rho_0)}{\rho_r - \rho_0} \end{cases} \tag{13}$$

If

$$\frac{q_2(\rho_0) - q_1(\rho_l)}{\rho_0 - \rho_l} \ge \frac{q_2(\rho_r) - q_2(\rho_0)}{\rho_r - \rho_0} \tag{14}$$

then

$$\rho(x,t) = \begin{cases} \rho_l, & \xi \le \frac{q_2(\rho_r)-q_1(\rho_l)}{\rho_r-\rho_l} \\ \rho_r, & \xi > \frac{q_2(\rho_r)-q_1(\rho_l)}{\rho_r-\rho_l} \end{cases} \tag{15}$$

2.2 Rarefaction wave: $\rho_l > \rho_r$

If $\rho_l > \rho_r$, and without loss of generality assume $\rho_l \ge \rho_0 + \varepsilon > \rho_0 \ge \rho_r$, then we construct the convex hull of the set $\{(\rho, y) : \rho_r \le \rho \le \rho_l \ \ and \ \ y \le q^\varepsilon(\rho)\}$. An illustration of the convex hull is shown in Figures 4 and 5 (the shaded region).

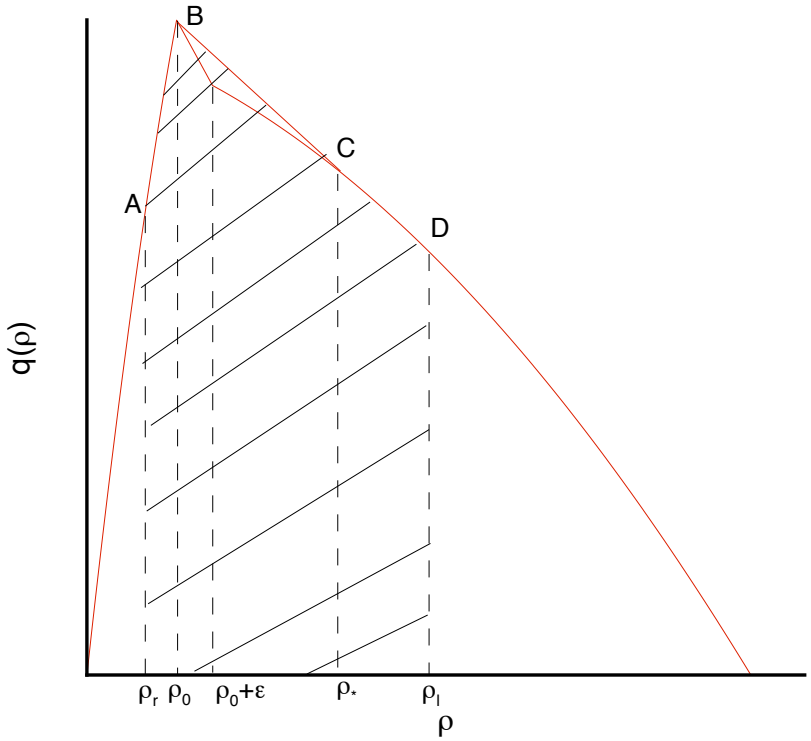

Figure 4: The convex hull of $\{(\rho, y) : \rho_r \le \rho \le \rho_l \ \ and \ \ y \le q^\varepsilon(\rho)\}$ for $(q_2^\varepsilon)'(\rho_l) < k_0^\varepsilon$.

If we look at the upper boundary of the convex hull in Figure 4, we can observe that it consists of a straight line segment from $(\rho_0, q^\varepsilon(\rho_0))$ to $(\rho_\star, q^\varepsilon(\rho_\star))$ (the line BC in the figure), and the two pieces of the curve $y = q^\varepsilon(\rho)$ for $\rho_r \le \rho \le \rho_0$ (AB in the figure) and $\rho_\star \le \rho \le \rho_l$ (CD in the figure), where BC is the tangent of $q^\varepsilon(\rho)$.

For the slope of BC, we have the relationship:

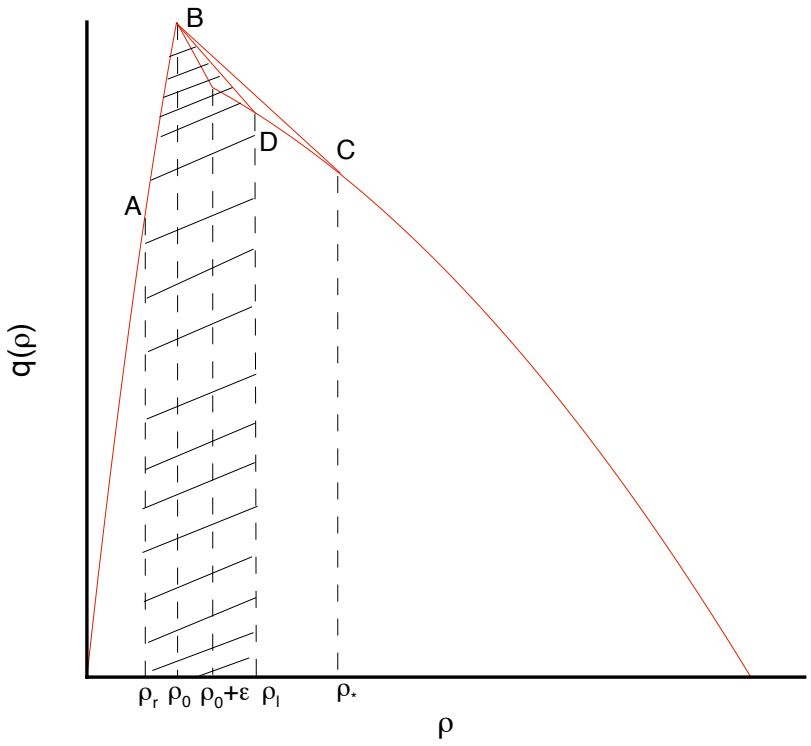

Figure 5: The convex hull of $\{(\rho, y) : \rho_r \le \rho \le \rho_l \ \ and \ \ y \le q^\varepsilon(\rho)\}$ for $(q_2^\varepsilon)'(\rho_l) \ge k_0^\varepsilon$.

$$\frac{q_2^\varepsilon(\rho_\star) - q_1(\rho_0)}{\rho_\star - \rho_0} = (q_2^\varepsilon)'(\rho_\star) = 2e_2'\rho_\star + e_1' \tag{16}$$

where $e_2' = e_2$, $e_1' = e_1 - 2\varepsilon e_2$ and $e_0' = e_0 + e_2\varepsilon^2 - e_1\varepsilon$. Then we can get a quadratic equation of $\rho_\star$. The discriminant of this quadratic equation

$$\Delta = 4e_2'[e_2'\rho_0^2 + e_1'\rho_0 + e_0' - (d_2\rho_0^2 + d_1\rho_0 + d_0)] > 0 \tag{17}$$

because $e_2' < 0$ and $e_2'\rho_0^2 + e_1'\rho_0 + e_0' < d_2\rho_0^2 + d_1\rho_0 + d_0$ when ε is small enough. The smaller root of (16) is just what we want.

Let $k_0^\varepsilon = (q_2^\varepsilon)'(\rho_\star) = 2e_2'\rho_\star + e_1'$. Apparently, $k_0^\varepsilon < (q_2^\varepsilon)'(\rho_0) = e_1' + 2e_2'\rho_0$. We can then obtain the entropy solution of the Riemann problem with the flux $q^\varepsilon(\rho)$ as follows, where $\xi = x/t$:

- If

$$(q_2^\varepsilon)'(\rho_l) < k_0^\varepsilon \tag{18}$$

as shown in Figure 4, then the solution is

$$\rho^\varepsilon(x,t) = \begin{cases} \rho_l, & \xi \le (q_2^\varepsilon)'(\rho_l) \\ \frac{\xi - e_1'}{2e_2'}, & (q_2^\varepsilon)'(\rho_l) < \xi \le k_0^\varepsilon \\ \rho_0, & k_0^\varepsilon < \xi \le q_1'(\rho_0) \\ \frac{\xi - d_1}{2d_2}, & q_1'(\rho_0) < \xi < q_1'(\rho_r) \\ \rho_r, & \xi \ge q_1'(\rho_r) \end{cases} \tag{19}$$

- If

$$(q_2^\varepsilon)'(\rho_l) \ge k_0^\varepsilon \tag{20}$$

as shown in Figure 5, then the solution is

$$\rho^\varepsilon(x,t) = \begin{cases} \rho_l, & \xi \le \frac{q_2^\varepsilon(\rho_l) - q_1(\rho_0)}{\rho_l - \rho_0} \\ \rho_0, & \frac{q_2^\varepsilon(\rho_l) - q_1(\rho_0)}{\rho_l - \rho_0} < \xi \le q_1'(\rho_0) \\ \frac{\xi - d_1}{2d_2}, & q_1'(\rho_0) < \xi < q_1'(\rho_r) \\ \rho_r, & \xi \ge q_1'(\rho_r) \end{cases} \tag{21}$$

Therefore, taking the limit $\varepsilon \to 0^+$, we have the following explicit solutions to the Riemann problem with the discontinuous flux (3), where k_0 is the value of k_0^ε with $\varepsilon = 0$:

- If

$$q_2'(\rho_l) < k_0 \tag{22}$$

then

$$\rho(x,t) = \begin{cases} \rho_l, & \xi \le q_2'(\rho_l) \\ \frac{\xi - e_1}{2e_2}, & q_2'(\rho_l) < \xi \le k_0 \\ \rho_0, & k_0 < \xi \le q_1'(\rho_0) \\ \frac{\xi - d_1}{2d_2}, & q_1'(\rho_0) < \xi < q_1'(\rho_r) \\ \rho_r, & \xi \ge q_1'(\rho_r) \end{cases} \tag{23}$$

If

$$q_2'(\rho_l) \ge k_0 \tag{24}$$

then

$$\rho(x,t) = \begin{cases} \rho_l, & \xi \le \frac{q_2(\rho_l) - q_1(\rho_0)}{\rho_l - \rho_0} \\ \rho_0, & \frac{q_2(\rho_l) - q_1(\rho_0)}{\rho_l - \rho_0} < \xi \le q_1'(\rho_0) \\ \frac{\xi - d_1}{2d_2}, & q_1'(\rho_0) < \xi < q_1'(\rho_r) \\ \rho_r, & \xi \ge q_1'(\rho_r) \end{cases} \tag{25}$$

3 Explicit construction of the entropy solutions

We now start the construction of explicit solutions to the conservation law (1) with such flows $q(\rho)$, when the initial condition is piecewise linear. We will first ignore the boundary conditions, and will leave the discussion of the treatment of piecewise constant boundary conditions to Sections 3.3 and 3.4. We begin with the generalized Riemann problem

$$\rho(x,0) = \begin{cases} \alpha_1 + \beta_1 x, & x < 0 \\ \alpha_2 + \beta_2 x, & x \geq 0 \end{cases} . \tag{26}$$

We also assume that, for the x range we are considering, the initial density $\alpha_i + \beta_i x$ is completely contained in one of the regimes $\rho \leq \rho_0$ or $\rho \geq \rho_0$ for $i = 1$ and 2. This does not lose generality, as we can break a single linear function into two pieces as in (26) when it crosses the critical density ρ_0. We also remark that we do not need to consider the case when both linear functions $\alpha_i + \beta_i x$, for $i = 1, 2$, are contained in a single regime $\rho \leq \rho_0$ or $\rho \geq \rho_0$, because this is covered by the results in (Wong and Wong, 2002b).

As in (Wong and Wong, 2002b and Lu et al., 2006), we will use heavily the following simple fact: for the scalar conservation law (1) with a quadratic flux $q(\rho) = a + b\rho + c\rho^2$ and a linear initial condition $\rho(x,0) = \alpha + \beta x$, the solution stays linear

$$\rho(x,t) = \alpha(t) + \beta(t)\, x \tag{27}$$

with

$$\alpha(t) = \frac{\alpha - b\beta t}{1 + 2c\beta t}, \qquad \beta(t) = \frac{\beta}{1 + 2c\beta t}. \tag{28}$$

This simple fact is the main reason that enables us to obtain explicit formulas for the entropy solution. The solution for each linear piece of the initial condition is given by (27)-(28) until neighboring waves interact with each other.

We now assume that the x-axis is divided into a number of elements, within each of which the initial density is given by a linear function $\rho(x,0) = \alpha + \beta x$ that is completely contained in one of the regimes $\rho \leq \rho_0$ or $\rho \geq \rho_0$. We consider the solution to the generalized Riemann problem with the two piecewise linear initial conditions. The left and right elements to the

inner boundary point under consideration are denoted by

$$\mathbf{e} = (x_l, x_r), \qquad \overline{\mathbf{e}} = (\overline{x}_l, \overline{x}_r)$$

respectively, with clearly $x_r = \overline{x}_l$. The initial condition density values at the relevant element boundaries are denoted by

$$\rho_l = \rho(x_l^+, 0), \quad \rho_r = \rho(x_r^-, 0); \qquad \overline{\rho}_l = \rho(\overline{x}_l^+, 0), \quad \overline{\rho}_r = \rho(\overline{x}_r^-, 0)$$

We also denote the densities in the left and right elements by $\rho_1(x,t)$ and $\rho_2(x,t)$, respectively, where

$$\rho_1(x,t) = \alpha_1(t) + \beta_1(t)x, \qquad \rho_2(x,t) = \alpha_2(t) + \beta_2(t)x.$$

We discuss the situation for rarefaction waves in Section 3.1 and the situation for shocks in Section 3.2. In Sections 3.3 and 3.4 we discuss the piecewise constant left and right boundary conditions, respectively. At last we provide the solution procedure in Section 3.5.

3.1 Case I: $\rho_r \geq \rho_0 \geq \overline{\rho}_l$

The elements $\mathbf{e}$ and $\overline{\mathbf{e}}$ belong to Flux II and Flux I in (4), respectively. Denote

$$k_0 = e_1 + 2e_2\rho_0 + 2e_2\sqrt{\frac{q_2(\rho_0) - q_1(\rho_0)}{e_2}} \tag{29}$$

We have the following two sub-cases.

3.1.1 Sub-case I (a): $q_2'(\rho_r) \leq k_0$

In this sub-case three new elements $\mathbf{e}_1$, $\mathbf{e}_2$ and $\mathbf{e}_3$ are created at the time $t = \Delta t$, as shown in Figure 6. We again consider only the time Δt smaller than the smallest time when the waves (characteristic lines or shocks) from the initial condition intersect with one another. The coordinates of the four nodes serving as the end points of the three elements $\mathbf{e}_1$, $\mathbf{e}_2$ and $\mathbf{e}_3$ at time Δt can be determined as

$$x_1(\Delta t) = x_r + q_2'(\rho_r)\Delta t, \qquad x_2(\Delta t) = x_r + k_0\Delta t$$

$$x_3(\Delta t) = x_r + q_1'(\rho_0)\Delta t, \qquad x_4(\Delta t) = x_r + q_1'(\overline{\rho}_l)\Delta t$$

The density at these end points at time Δt are given by

$$\rho(x_1(\Delta t), \Delta t) = \rho_r, \qquad \rho(x_2(\Delta t)^-, \Delta t) = \frac{k_0 - e_1}{2e_2}, \qquad \rho(x_2(\Delta t)^+, \Delta t) = \rho_0,$$

$$\rho(x_3(\Delta t), \Delta t) = \rho_0, \qquad \rho(x_4(\Delta t), \Delta t) = \overline{\rho}_l$$

and the density is linear within each of the new elements $\mathbf{e}_i$, $i = 1, 2, 3$. In particular, the density within $\mathbf{e}_2$ is a constant $\rho = \rho_0$.

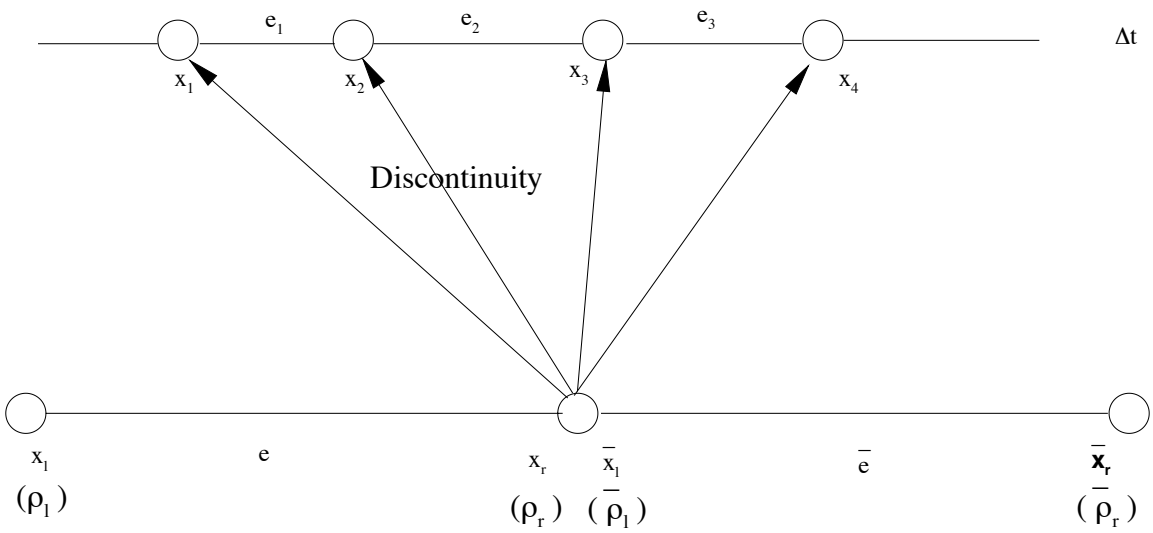

Figure 6: Sub-case I (a): $q_2'(\rho_r) \leq k_0$.

3.1.2 Sub-case I (b): $q_2'(\rho_r) > k_0$

In this sub-case, the situation is shown in Figure 7. The discontinuity which is generated from the point $x_r = \overline{x}_l$ will move to the right or left along a curve. If the discontinuity moves to the left, an easy way to determine the location of the discontinuity $\overline{x}_l + \Delta x$ after time Δt is through conservation in the rectangular region Ω with $(\overline{x}_l + \Delta x, 0)$ and $(\overline{x}_l + q_1'(\overline{\rho}_l)\Delta t, \Delta t)$ as the end points of a diagonal (see Figure 7).

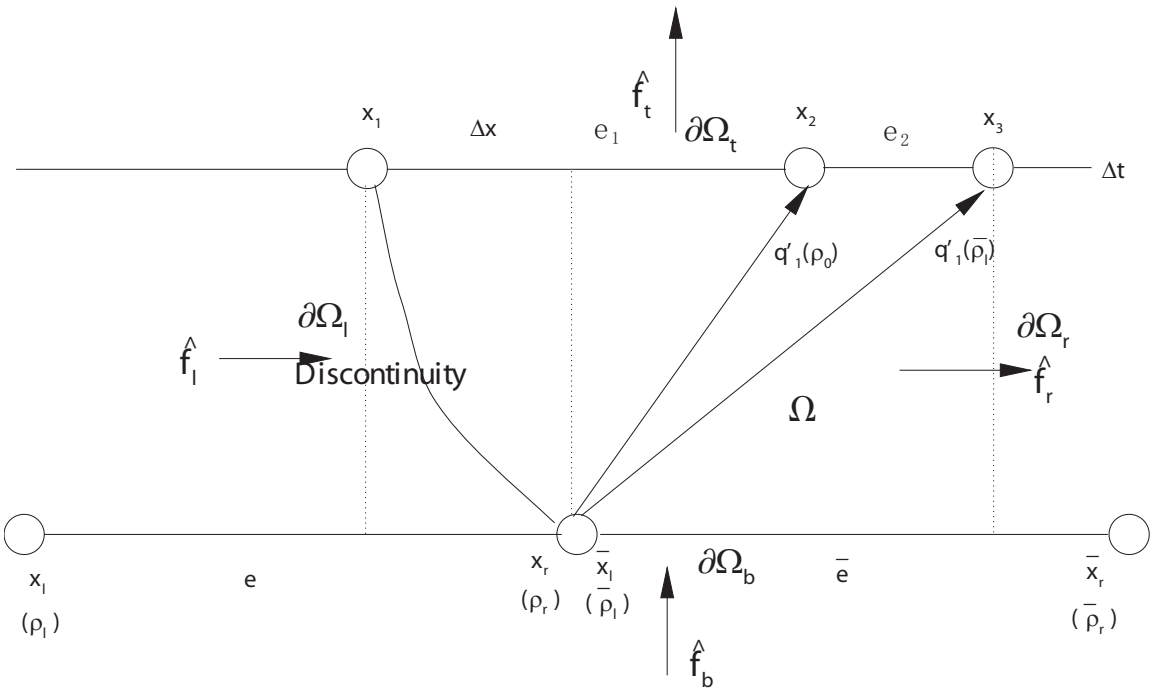

Figure 7: Sub-case I (b): $q_2'(\rho_r) > k_0$.

The flux at the left boundary $\partial\Omega_l$, namely the number of vehicles coming from the left

boundary into the region Ω during time period Δt is

$$\hat{f}_l = \int_0^{\Delta t} q_2|_{x=x_r+\Delta x}\, dt = \int_0^{\Delta t} \{e_0+e_1[\alpha_1(t)+\beta_1(t)(x_r+\Delta x)]+e_2[\alpha_1(t)+\beta_1(t)\,(x_r+\Delta x)]^2\}\, dt \tag{30}$$

Likewise, the flux at the right boundary $\partial\Omega_r$, namely the number of vehicles leaving the right boundary from the region Ω is

$$\begin{aligned} \hat{f}_r &= \int_0^{\Delta t} q_1|_{x=\overline{x}_l+q_1'(\overline{\rho}_l)\Delta t}\, dt \qquad (31)\\ &= \int_0^{\Delta t} \{d_0 + d_1[\alpha_2(t) + \beta_2(t)(\overline{x}_l + q_1'(\overline{\rho}_l)\Delta t)] + d_2[\alpha_2(t) + \beta_2(t)(\overline{x}_l + q_1'(\overline{\rho}_l)\Delta t)]^2\}\, dt. \end{aligned}$$

The initial number of vehicles within the region Ω at time $t = 0$ is

$$\hat{f}_b = \int_{x_r+\Delta x}^{x_r} (\alpha_1(0) + \beta_1(0)x)\, dx + \int_{\overline{x}_l}^{\overline{x}_l+q_1'(\overline{\rho}_l)\Delta t} (\alpha_2(0) + \beta_2(0)x)\, dx \tag{32}$$

and the final number of vehicles within the region Ω at time t=Δt is

$$\hat{f}_t = \int_{x_r+\Delta x}^{\overline{x}_l+q_1'(\rho_0)\Delta t} \rho_0\, dx + \int_{\overline{x}_l+q_1'(\rho_0)\Delta t}^{\overline{x}_l+q_1'(\overline{\rho}_l)\Delta t} (\alpha_2(\Delta t) + \beta_2(\Delta t)x)\, dx. \tag{33}$$

From the flow conservation principle, we deduce that

$$\hat{f}_l - \hat{f}_r + \hat{f}_b - \hat{f}_t = 0. \tag{34}$$

We then obtain from (34) the explicit equation determining Δx as

$$F_1(\Delta t)\Delta x^2 + F_2(\Delta t)\Delta x + F_3(\Delta t) = 0 \tag{35}$$

where

$$\begin{aligned} F_1(\Delta t) &= \rho_l - \rho_r \\ F_2(\Delta t) &= -2[e_1(\rho_l - \rho_r)\Delta t + 2e_2\rho_0(\rho_l - \rho_r)\Delta t + (\rho_0 - \rho_r)(x_l - x_r)] \\ F_3(\Delta t) &= \Delta t\{e_1^2(\rho_l - \rho_r)\Delta t + 2e_1\rho_r(x_r - x_l) + 2\{-2e_0e_2\rho_l\Delta t + 2d_1e_2\rho_0\rho_l\Delta t \\ &\quad +2d_2e_2\rho_0^2\rho_l\Delta t + 2e_0e_2\rho_r\Delta t - 2d_1e_2\rho_0\rho_r\Delta t - 2d_2e_2\rho_0^2\rho_r\Delta t - e_0x_l + d_1\rho_0x_l \\ &\quad +d_2\rho_0^2x_l - e_2\rho_r^2x_l + d_0[2e_2(\rho_l - \rho_r)\Delta t + x_l - x_r] + [e_0 - \rho_0(d_1 + d_2\rho_0) + e_2\rho_r^2]x_r\}\} \end{aligned}$$

The discontinuity trajectory can therefore be determined by solving the quadratic equation (35). Then when $F_1(\Delta t) \neq 0$,

$$\Delta x = \frac{-F_2(\Delta t) - \sqrt{\Delta}}{2F_1(\Delta t)} \tag{36}$$

where $\Delta = F_2(\Delta t)^2 - 4F_1(\Delta t)F_3(\Delta t)$. If the root Δx is positive, then the assumption of a left-moving discontinuity is incorrect. We can then repeat the procedure above assuming that the discontinuity is right-moving. It turns out that the formula for the location Δx of the discontinuity is still given by (36). Therefore, we do not need to distinguish whether the discontinuity moves to the left or right. The coordinates of the three nodes serving as the end points of the three elements $\mathbf{e}_1$ and $\mathbf{e}_2$ at time Δt can be determined as

$$x_1(\Delta t) = x_r + \Delta x(\Delta t), \qquad x_2(\Delta t) = x_r + q_1'(\rho_0)\Delta t, \qquad x_3(\Delta t) = x_r + q_1'(\overline{\rho}_l)\Delta t.$$

The density at these end points at time Δt are given by

$$\rho(x_1(\Delta t)^+, \Delta t) = \rho_0, \quad \rho(x_2(\Delta t), \Delta t) = \rho_0, \quad \rho(x_3(\Delta t), \Delta t) = \overline{\rho}_l$$

and the density is linear within each of the new elements $\mathbf{e}_i$, $i = 1, 2$. In particular, the density within $\mathbf{e}_1$ is a constant $\rho = \rho_0$.

3.2 Case II: $\rho_r \leq \rho_0 \leq \overline{\rho}_l$

In this case the elements $\mathbf{e}$ and $\overline{\mathbf{e}}$ belonging to Flux I and Flux II in (4), respectively. We have the following two sub-cases.

3.2.1 Sub-case II (a): $\rho_r < \rho_0$

(i) If

$$\frac{q_1(\rho_r) - q_2(\rho_0)}{\rho_r - \rho_0} \geq \frac{q_2(\overline{\rho}_l) - q_2(\rho_0)}{\overline{\rho}_l - \rho_0}$$

then a shock satisfying the Lax entropy condition (Lax, 1973) is generated from the point $x_r = \overline{x}_l$ and will move to the right or left along a curve determined by the Rankine-Hugoniot jump condition. If the shock moves to the right, as shown in Figure 8, an easy way to determine the location of the shock $\overline{x}_l + \Delta x$ after time Δt is through conservation in the

rectangular region Ω with $(\overline{x}_l, 0)$ and $(\overline{x}_l + \Delta x, \Delta t)$ as the end points of a diagonal (see Figure 8). Notice that, since we consider only the time Δt smaller than the smallest time when the waves (characteristic lines or shocks) from the initial condition intersect with one another, we can safely assume that the left and top boundaries of this rectangle, $\partial\Omega_l$ and $\partial\Omega_t$, belong to Flux I, and the right and bottom boundaries of this rectangle, $\partial\Omega_r$ and $\partial\Omega_b$, belong to Flux II.

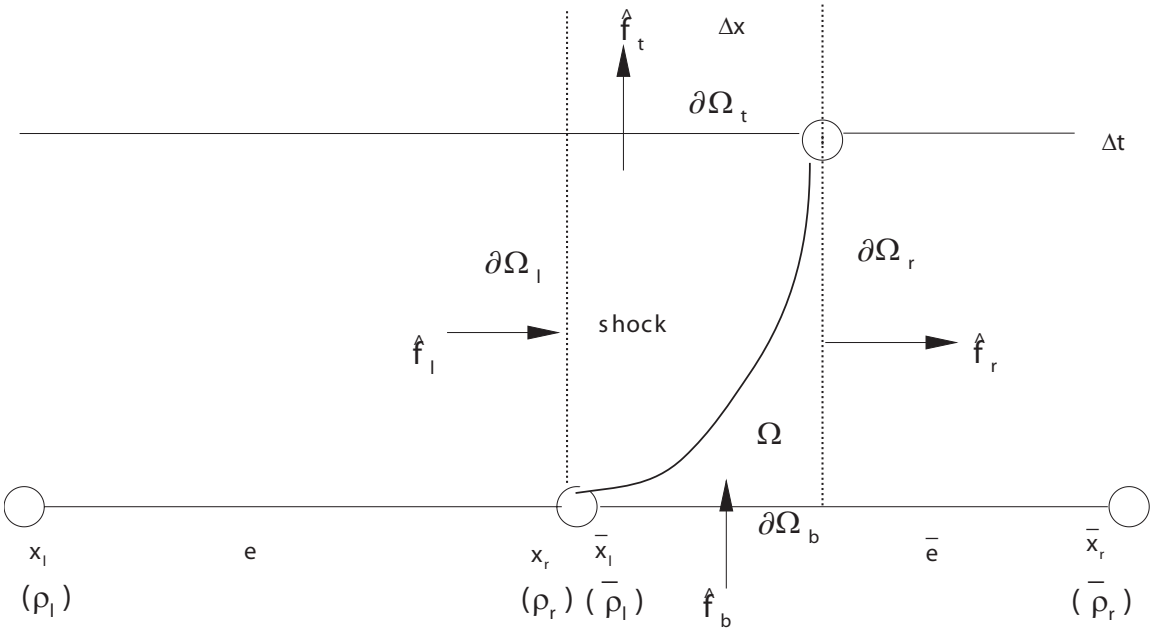

Figure 8: Sub-case II (a) (i): $\rho_r < \rho_0$ and $\frac{q_1(\rho_r)-q_2(\rho_0)}{\rho_r-\rho_0} \geq \frac{q_2(\overline{\rho}_l)-q_2(\rho_0)}{\overline{\rho}_l-\rho_0}$.

The flux at the left boundary $\partial\Omega_l$, namely the number of vehicles coming from the left boundary into the region Ω during time period Δt is

$$\hat{f}_l = \int_0^{\Delta t} q_1|_{x=x_r}\, dt = \int_0^{\Delta t} \left[d_0 + d_1(\alpha_1(t) + \beta_1(t)\, x_r) + d_2(\alpha_1(t) + \beta_1(t)\, x_r)^2\right]\, dt \qquad (37)$$

Likewise, the flux at the right boundary $\partial\Omega_r$, namely the number of vehicles leaving the right boundary from the region Ω is

$$\begin{aligned}\hat{f}_r &= \int_0^{\Delta t} q_2|_{x=\overline{x}_l+\Delta x}\, dt \\ &= \int_0^{\Delta t} \left[e_0 + e_1(\alpha_2(t)+\beta_2(t)(\overline{x}_l+\Delta x)) + e_2(\alpha_2(t)+\beta_2(t)(\overline{x}_l+\Delta x))^2\right] dt. \quad (38)\end{aligned}$$

The initial number of vehicles within the region Ω at time $t = 0$ is

$$\hat{f}_b = \int_{\overline{x}_l}^{\overline{x}_l+\Delta x} (\alpha_2(0)+\beta_2(0)x)\, dx \quad (39)$$

and the final number of vehicles within the region Ω at time $t = \Delta t$ is

$$\hat{f}_t = \int_{x_r}^{x_r+\Delta x} (\alpha_1(\Delta t)+\beta_1(\Delta t)x)\, dx. \quad (40)$$

From the flow conservation principle, we deduce that

$$\hat{f}_l - \hat{f}_r + \hat{f}_b - \hat{f}_t = 0. \quad (41)$$

We obtain the explicit equation determining Δx by

$$F_1(\Delta t)\,\Delta x^2 + F_2(\Delta t)\,\Delta x + F_3(\Delta t) = 0 \quad (42)$$

where

$$\begin{aligned}F_1(\Delta t) &= 2\Delta t(d_2-e_2)(\rho_r-\rho_l)(\overline{\rho}_r-\overline{\rho}_l) + (x_r-x_l)(\overline{\rho}_r-\overline{\rho}_l) - (\overline{x}_r-\overline{x}_l)(\rho_r-\rho_l) \\ F_2(\Delta t) &= 2\{-(x_l-x_r)[\Delta t(e_1+2e_2\rho_r)(\overline{\rho}_l-\overline{\rho}_r) - (\overline{\rho}_l-\rho_r)(\overline{x}_l-\overline{x}_r)] + d_1\Delta t(\rho_l-\rho_r)[2e_2\Delta t(\overline{\rho}_l-\overline{\rho}_r) \\ &\quad +\overline{x}_l-\overline{x}_r] - 2d_2\Delta t(\rho_l-\rho_r)[\Delta t e_1(\overline{\rho}_l-\overline{\rho}_r) - \overline{\rho}_l(\overline{x}_l-\overline{x}_r)]\} \\ F_3(\Delta t) &= \Delta t\{(x_l-x_r)\{\Delta t[e_1^2+4(d_0-e_0)e_2](\overline{\rho}_l-\overline{\rho}_r) + 2(d_0-e_0-e_1\overline{\rho}_l-e_2\overline{\rho}_l^2)(\overline{x}_l-\overline{x}_r)\} \\ &\quad +2d_2\{\Delta t^2[e_1^2+4(d_0-e_0)e_2](\rho_l-\rho_r)(\overline{\rho}_l-\overline{\rho}_r) + 2\Delta t\{e_2[\overline{\rho}_l\rho_r^2(x_l-x_r) + \rho_r^2\overline{\rho}_r(x_r-x_l) \\ &\quad -\overline{\rho}_l^2(\rho_l-\rho_r)(\overline{x}_l-\overline{x}_r)] + (d_0-e_0-e_1\overline{\rho}_l)(\rho_l-\rho_r)(\overline{x}_l-\overline{x}_r)\} + \rho_r^2(x_l-x_r)(\overline{x}_l-\overline{x}_r)\} \\ &\quad -d_1^2\Delta t(\rho_l-\rho_r)[2\Delta t e_2(\overline{\rho}_l-\overline{\rho}_r) + \overline{x}_l-\overline{x}_r] + 2d_1\rho_r(x_l-x_r)(2\Delta t e_2(\overline{\rho}_l-\overline{\rho}_r) + \overline{x}_l-\overline{x}_r)\}\end{aligned}$$

The shock trajectory can therefore be determined by solving the quadratic equation (42). If $F_1(\Delta t) \neq 0$, then

$$\Delta x = \frac{-F_2(\Delta t) + \sqrt{\Delta}}{2F_1(\Delta t)} \tag{43}$$

where $\Delta = F_2(\Delta t)^2 - 4F_1(\Delta t)F_3(\Delta t)$. If the root Δx is negative, then the assumption of a right-moving shock is incorrect. However, as before, it turns out that the formula (43) is still valid in this case.

(ii) If, on the other hand,

$$\frac{q_1(\rho_r) - q_2(\rho_0)}{\rho_r - \rho_0} < \frac{q_2(\overline{\rho}_l) - q_2(\rho_0)}{\overline{\rho}_l - \rho_0}$$

then two shocks satisfying the Lax entropy condition are generated from the point $x_r = \overline{x}_l$ and one new element $\mathbf{e}_1$ is created at the time $t = \Delta t$, as shown in Figure 9. We again consider only the time Δt smaller than the smallest time when the waves (characteristic lines or shocks) from the initial condition intersect with one another.

By the Rankine-Hugoniot jump condition

$$\Delta x_2'(\Delta t) = \frac{q_2(\alpha_2(\Delta t) + \beta_2(\Delta t)(\overline{x}_l + \Delta x_2(\Delta t))) - q_2(\rho_0)}{\alpha_2(\Delta t) + \beta_2(\Delta t)(\overline{x}_l + \Delta x_2(\Delta t)) - \rho_0} \tag{44}$$

If $\overline{\rho}_l \neq \overline{\rho}_r$, then

$$\begin{aligned}\Delta x_2(\Delta t) = {} & [e_1(\overline{\rho}_l - \overline{\rho}_r)\Delta t\sqrt{\overline{x}_r - \overline{x}_l} + 2e_2\rho_0(\overline{\rho}_l - \overline{\rho}_r)\Delta t\sqrt{\overline{x}_r - \overline{x}_l} \\ & + (\sqrt{\overline{x}_r - \overline{x}_l} - \sqrt{2e_2(\overline{\rho}_r - \overline{\rho}_l)\Delta t + \overline{x}_r - \overline{x}_l})(\rho_0\overline{x}_l - \overline{\rho}_r\overline{x}_l - \rho_0\overline{x}_r + \overline{\rho}_l\overline{x}_r)]/[(\overline{\rho}_l - \overline{\rho}_r)\sqrt{\overline{x}_r - \overline{x}_l}]\end{aligned} \tag{45}$$

If $\overline{\rho}_l = \overline{\rho}_r$, then

$$\Delta x_2(\Delta t) = [e_1 + e_2(\overline{\rho}_l + \rho_0)]\Delta t \tag{46}$$

The flux at the left boundary $\partial\Omega_l$, namely the number of vehicles coming from the left boundary into the region Ω during time period Δt is

$$\tilde{f}_l = \int_0^{\Delta t} q_1|_{x=x_r}\, dt = \int_0^{\Delta t} \left[d_0 + d_1(\alpha_1(t) + \beta_1(t)\, x_r) + d_2(\alpha_1(t) + \beta_1(t)\, x_r)^2\right]\, dt \tag{47}$$

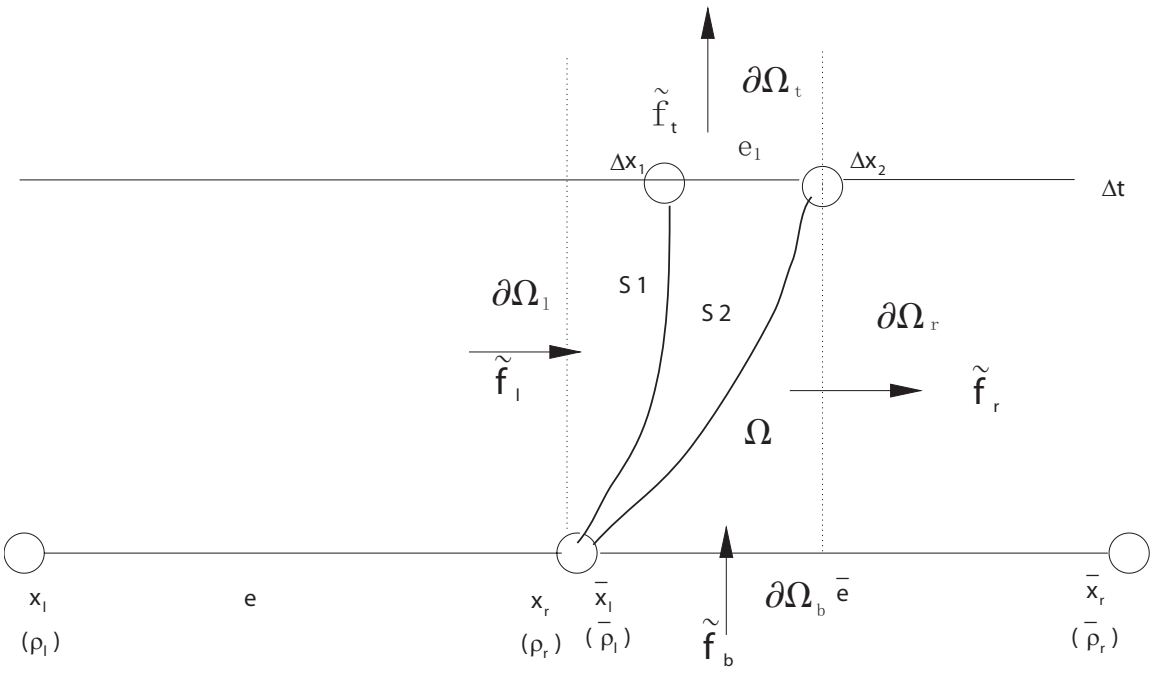

Figure 9: Sub-case II (a) (ii): $\rho_r < \rho_0$ and $\frac{q_1(\rho_r)-q_2(\rho_0)}{\rho_r-\rho_0} < \frac{q_2(\overline{\rho}_l)-q_2(\rho_0)}{\overline{\rho}_l-\rho_0}$.

The flux at the right boundary $\partial\Omega_r$, namely the number of vehicles leaving the right boundary from the region Ω is

$$\begin{aligned}\tilde{f}_r &= \int_0^{\Delta t} q_2|_{x=\overline{x}_l+\Delta x_2}\, dt \\ &= \int_0^{\Delta t} \left[e_0 + e_1(\alpha_2(t)+\beta_2(t)(\overline{x}_l+\Delta x_2)) + e_2(\alpha_2(t)+\beta_2(t)(\overline{x}_l+\Delta x_2))^2\right]\, dt. \quad (48)\end{aligned}$$

The initial number of vehicles within the region Ω at time $t = 0$ is

$$\tilde{f}_b = \int_{\overline{x}_l}^{\overline{x}_l+\Delta x_2} (\alpha_2(0)+\beta_2(0)x)\, dx \quad (49)$$

and the final number of vehicles within the region Ω at time

$$\tilde{f}_t = \int_{x_r}^{x_r+\Delta x_1} (\alpha_1(\Delta t) + \beta_1(\Delta t)x)\, dx + \int_{x_r+\Delta x_1}^{x_r+\Delta x_2} (\rho_0)\, dx \tag{50}$$

From the flow conservation principle, we deduce that

$$\tilde{f}_l - \tilde{f}_r + \tilde{f}_b - \tilde{f}_t = 0. \tag{51}$$

From this, we obtain the explicit equation determining Δx_1 as

$$\tilde{F}_1(\Delta t)\, {\Delta x_1}^2 + \tilde{F}_2(\Delta t)\, \Delta x_1 + \tilde{F}_3(\Delta t) = 0 \tag{52}$$

where

$$\begin{aligned}
\tilde{F}_1(\Delta t) &= (\rho_r - \rho_l)[2e_2(\overline{\rho}_l - \overline{\rho}_r)\Delta t + \overline{x}_l - \overline{x}_r] \\
\tilde{F}_2(\Delta t) &= 2[d_1(\rho_l - \rho_r)\Delta t + 2d_2\rho_0(\rho_l - \rho_r)\Delta t + (\rho_0 - \rho_r)(x_l - x_r)][2e_2(\overline{\rho}_l - \overline{\rho}_r)\Delta t + \overline{x}_l - \overline{x}_r] \\
\tilde{F}_3(\Delta t) &= 2d_1\rho_r\Delta t(x_l - x_r)[2e_2(\overline{\rho}_l - \overline{\rho}_r)\Delta t + \overline{x}_l - \overline{x}_r] + d_1^2(\rho_l - \rho_r)\Delta t^2[2e_2(\overline{\rho}_r - \overline{\rho}_l)\Delta t + \overline{x_r} - \overline{x}_l] + \\
&\quad (x_l - x_r)\{\Delta t\{e_1^2(\overline{\rho}_l - \overline{\rho}_r)\Delta t + 2e_1\overline{\rho}_l(\overline{x}_r - \overline{x}_l) + 2\{d_0[2e_2(\overline{\rho}_l - \overline{\rho}_r)\Delta t + \overline{x}_l - \overline{x}_r] \\
&\quad + e_2\overline{\rho}_l^2(\overline{x}_r - \overline{x}_l) + e_0[2e_2(\overline{\rho}_r - \overline{\rho}_l)\Delta t + \overline{x}_r - \overline{x}_l]\}\} - 2[e_1(\overline{\rho}_l - \overline{\rho}_r)\Delta t + 2e_2\rho_0(\overline{\rho}_l - \overline{\rho}_r)\Delta t \\
&\quad + (\rho_0 - \overline{\rho}_l)(\overline{x}_l - \overline{x}_r)]\Delta x_2(\Delta t) + (\overline{\rho}_l - \overline{\rho}_r)\Delta x_2(\Delta t)^2\} \\
&\quad + 2d_2\Delta t\{[e_1^2 + 4(d_0 - e_0)e_2](\rho_l - \rho_r)(\overline{\rho}_l - \overline{\rho}_r)\Delta t^2 + 2\{e_2[\overline{\rho}_l\rho_r^2(x_l - x_r) + \rho_r^2\overline{\rho}_r^2(x_r - x_l) \\
&\quad - \overline{\rho}_l^2(\rho_l - \rho_r)(\overline{x}_l - \overline{x}_r)] + (d_0 - e_0)(\rho_l - \rho_r)(\overline{x}_l - \overline{x}_r)\}\Delta t + \rho_r^2(x_l - x_r)(\overline{x}_l - \overline{x}_r) \\
&\quad + 2(\rho_l - \rho_r)[2e_2\rho_0(\overline{\rho}_r - \overline{\rho}_l)\Delta t - (\rho_0 - \overline{\rho}_l)(\overline{x}_l - \overline{x}_r)]\Delta x_2(\Delta t) \\
&\quad + (\rho_l - \rho_r)(\overline{\rho}_l - \overline{\rho}_r)\Delta x_2(\Delta t)^2 - 2e_1(\rho_l - \rho_r)\Delta t[-\overline{\rho}_r\Delta x_2(\Delta t) + \overline{\rho}_l(\overline{x}_l - \overline{x}_r + \Delta x_2(\Delta t))]\}
\end{aligned}$$

Therefore, when $\tilde{F}_1(\Delta t) \neq 0$,

$$\Delta x_1 = \frac{-\tilde{F}_2(\Delta t) + \sqrt{\Delta}}{2\tilde{F}_1(\Delta t)} \tag{53}$$

with $\Delta = \tilde{F}_2(\Delta t)^2 - 4\tilde{F}_1(\Delta t)\tilde{F}_3(\Delta t)$.

It is easy to find that the density within $\mathbf{e}_1$ is a constant $\rho = \rho_0$.

We can verify again that the formulas for the location Δx_1 and Δx_2 of the two shocks stay the same regardless of whether the two shocks move to the left or right.

3.2.2 Sub-case II (b): $\rho_r = \rho_0$

In this sub-case, if $\rho_l = \rho_r$, then one shock satisfying the Lax entropy condition is generated from the point $x_r = \overline{x}_l$, as shown in Figure 8. The formula for the location Δx of the shock is the same as that given in (43).

If $\rho_l \neq \rho_r$, then two shocks satisfying the Lax entropy condition are generated from the point $x_r = \overline{x}_l$, as shown in Figure 9. The formulas for the locations Δx_1 and Δx_2 of the two shocks are given by (53) and (45).

3.3 Boundary conditions from the highway entrance

We now consider the boundary condition at the left boundary $x = 0$, which is the highway entrance. Looking at the solution (27)-(28), we can see that the general solution with a linear initial condition is not linear in t for fixed x, unless $\beta = 0$, in which case the solution is constant in t. Therefore, within our piecewise linear (in space) framework, we can only consider piecewise constant boundary conditions.

We use the same notation as used previously. The interface is at $x_r = \overline{x}_l = 0$, and the left density value ρ_r at $x = 0$ is given by the boundary condition. Otherwise, this is identical to the situation studied in the two previous cases for an internal generalized Riemann problem. Again, we would need to consider the situation where ρ_r and the linear function in the first element with end values $\overline{\rho}_l$ and $\overline{\rho}_r$ belong to different regimes in (4), for otherwise the solution is the one obtained in (Wong and Wong, 2002b).

3.3.1 Sub-case B (a): $\rho_r \leq \rho_0 \leq \overline{\rho}_l$

If $\rho_r \leq \rho_0 \leq \overline{\rho}_l$, one or two shocks are generated. We consider only the situation that the shock moves to the right.

(i) $\rho_r < \rho_0$

If

$$\frac{q_1(\rho_r) - q_2(\rho_0)}{\rho_r - \rho_0} \geq \frac{q_2(\overline{\rho}_l) - q_2(\rho_0)}{\overline{\rho}_l - \rho_0},$$

a shock is generated and its location Δx after time Δt is given by (42), except that the left flux $\hat{f}_l$ given by (37) is simplified to

$$\hat{f}_l = q_1(\rho_r)\,\Delta t$$

and the top flux $\hat{f}_t$ given by (40) is simplified to

$$\hat{f}_t = \rho_r\,\Delta x.$$

Therefore, the coefficients in the quadratic equation (43) which determines the shock location Δx are simplified to

$$\begin{aligned} F_1(\Delta t) &= \overline{\rho}_r - \overline{\rho}_l \\ F_2(\Delta t) &= 2[e_1(\overline{\rho}_l - \overline{\rho}_r)\Delta t + 2e_2\rho_r(\overline{\rho}_l - \overline{\rho}_r)\Delta t + (\rho_r - \overline{\rho}_l)(\overline{x}_l - \overline{x}_r)] \\ F_3(\Delta t) &= -\Delta t\{[e_1^2 + 4(d_0 - e_0)e_2](\overline{\rho}_l - \overline{\rho}_r)\Delta t + 2(d_0 - e_0 - e_1\overline{\rho}_l - e_2\overline{\rho}_l^2)(\overline{x}_l - \overline{x}_r) \\ &\quad +2d_1\rho_r[2e_2(\overline{\rho}_l - \overline{\rho}_r)\Delta t + \overline{x}_l - \overline{x}_r] + 2d_2\rho_r^2[2e_2(\overline{\rho}_l - \overline{\rho}_r)\Delta t + \overline{x}_l - \overline{x}_r]\}. \end{aligned} \tag{54}$$

On the other hand, if

$$\frac{q_1(\rho_r) - q_2(\rho_0)}{\rho_r - \rho_0} < \frac{q_2(\overline{\rho}_l) - q_2(\rho_0)}{\overline{\rho}_l - \rho_0},$$

two shocks are generated and their locations Δx_1 and Δx_2 after time Δt are given by (53) and (45), except that the left flux $\tilde{f}_l$ given by (47) is simplified to

$$\tilde{f}_l = q_1(\rho_r)\,\Delta t$$

and the top flux $\tilde{f}_t$ given by (50) is simplified to

$$\tilde{f}_t = \rho_r\,\Delta x_1 + \rho_0\,(\Delta x_2 - \Delta x_1).$$

Therefore, the coefficients in the quadratic equation (52) which determines the shock location

Δx_1 are simplified to

$$\begin{aligned}
\tilde{F}_1(\Delta t) &= 0 \\
\tilde{F}_2(\Delta t) &= 2(\rho_r - \rho_0)[2e_2(\overline{\rho}_l - \overline{\rho}_r)\Delta t + \overline{x}_l - \overline{x}_r] \\
\tilde{F}_3(\Delta t) &= -\Delta t\{2\rho_r(d1 + d_2\rho_r)[2e_2(\overline{\rho}_l - \overline{\rho}_r)\Delta t + \overline{x}_l - \overline{x}_r] + e_1^2(\overline{\rho}_l - \overline{\rho}_r)\Delta t \\
&\quad +2e_1\overline{\rho}_l(\overline{x}_r - \overline{x}_l) + 2\{d_0[2e_2(\overline{\rho}_l - \overline{\rho}_r)\Delta t + \overline{x}_l - \overline{x}_r] + e_2\overline{\rho}_l^2(\overline{x}_r - \overline{x}_l) + \\
&\quad e_0[2e_2(\overline{\rho}_r - \overline{\rho}_l)\Delta t - \overline{x}_l + \overline{x}_r]\}\} + 2[e_1(\overline{\rho}_l - \overline{\rho}_r)\Delta t + 2e_2\rho_0(\overline{\rho}_l - \overline{\rho}_r)\Delta t \\
&\quad +(\rho_0 - \overline{\rho}_l)(\overline{x}_l - \overline{x}_r)]\Delta x_2 + (\overline{\rho}_r - \overline{\rho}_l)\Delta x_2^2
\end{aligned}$$

(ii) $\rho_r = \rho_0$

In this case a shock is generated and the coefficients in the quadratic equation (43) which determines the shock location Δx are the same as those in (54).

3.3.2 Sub-case B (b): $\rho_r \geq \rho_0 \geq \overline{\rho}_l$

If $\rho_r \geq \rho_0 \geq \overline{\rho}_l$, a rarefaction wave is formed. We still use the notation introduced previously. The interface is at $x_r = \overline{x}_l = 0$, and the left density value ρ_r at $x = 0$ is given by the boundary condition. Otherwise, this is identical to the situation studied in the two previous subsections for an internal generalized Riemann problem. Again, we would need to consider the situation where ρ_r and the linear function in the first element with end values $\overline{\rho}_l$ and $\overline{\rho}_r$ belong to different regimes in (4), for otherwise the solution is the one obtained in (Wong and Wong, 2002b).

(i) $q_2'(\rho_r) \leq k_0$. The formulas are the same as those given in Section 3.1.

(ii) $q_2'(\rho_r) > k_0$. In this case a discontinuity is generated and its location Δx after time Δt is given by (35), except that the left flux $\hat{f}_l$ given by (30) is changed to

$$\hat{f}_l = q_2(\rho_r)\,\Delta t,$$

the top flux $\hat{f}_t$ given by (33) is changed to

$$\hat{f}_t = \rho_r \Delta x + \rho_0 (q_1'(\overline{\rho}_0)\Delta t - \Delta x) + \int_{x_r + q_1'(\rho_0)\Delta t}^{x_r + q_1'(\overline{\rho}_l)\Delta t} (\alpha_2(\Delta t) + \beta_2(\Delta t)x)\, dx,$$

and the bottom flux $\hat{f}_b$ given by (32) is changed to

$$\hat{f}_b = \int_{x_r}^{x_r + q_1'(\overline{\rho}_l)\Delta t} (\alpha_2(\Delta t) + \beta_2(\Delta t)x)\, dx.$$

Therefore, the coefficients in the quadratic equation (35) which determines the shock location Δx are changed to

$$\begin{aligned} F_1(\Delta t) &= 0 \\ F_2(\Delta t) &= 2(\rho_0 - \rho_r) \\ F_3(\Delta t) &= -2[d_0 - e_0\rho_0(d_1 + d_2\rho_0) - \rho_r(e_1 + e_2\rho_r)]\Delta t. \end{aligned}$$

3.4 Boundary conditions for the highway exit

In this subsection we discuss the boundary condition at the right boundary $x = x_{end}$, which is the highway exit.

We consider a typical exit setup with a traffic signal, which alternates between green and red lights. This is similar to the piecewise constant boundary condition considered for the entrance in the previous subsection. The constant values of the density ρ for the green and red lights are $\overline{\rho}_l = 0$ and $\overline{\rho}_l = \rho_{\max}$, respectively.

When $\overline{\rho}_l = \rho_{\max}$, corresponding to the situation of a red light, a left-moving shock is formed. We again only consider the situation $\rho_r \le \rho_0 \le \overline{\rho}_l$, corresponding to the situation where the density at the left of x_{end} belongs to the regime of Flux I in (4).

The value Δx determining the shock location $x_{end} + \Delta x$ after time Δt (recall that in this case Δx is negative) is given by (43), except that the right flux $\hat{f}_r$ given by (38) is changed to

$$\hat{f}_r = 0,$$

the top flux $\hat{f}_t$ given by (40) is changed to

$$\hat{f}_t = \rho_{\max}\,\Delta x,$$

and the bottom flux $\hat{f}_b$ given by (39) is changed to

$$\hat{f}_b = \int_{x_r}^{x_r+\Delta x} (\alpha_1(0) + \beta_1(0)x)\,dx.$$

Therefore, the coefficients in the quadratic equation (42) which determines the shock location $x_{end} + \Delta x$ are simplified to

$$\begin{aligned}
F_1(\Delta t) &= \rho_l - \rho_r \\
F_2(\Delta t) &= -2[d_1(\rho_l - \rho_r)\Delta t + 2d_2\overline{\rho}_l(\rho_l - \rho_r)\Delta t + (\overline{\rho}_l - \rho_r)(x_l - x_r)] \\
F_3(\Delta t) &= \Delta t\{d_1^2(\rho_l - \rho_r)\Delta t + 2d_1\rho_r(-x_l + x_r) - 2\{-[e_0 + \overline{\rho}_l(e_1 + e_2\overline{\rho}_l)](x_l - x_r) \\
&\quad + d_0[2d_2(\rho_l - \rho_r)\Delta t + x_l - x_r] + d_2[-2e_2\rho_l\overline{\rho}_l^2\Delta t + 2e_2\overline{\rho}_l^2\rho_r\Delta t + 2e_0(\rho_r - \rho_l)\Delta t \\
&\quad + 2e_1\overline{\rho}_l(\rho_r - \rho_l)\Delta t + \rho_r^2 x_l - \rho_r^2 x_r]\}\}
\end{aligned}$$

When $\overline{\rho}_l = 0$, corresponding to the situation of a green light, a rarefaction wave is formed. The formulas are the same as those given in Section 3.1.1.

We can also easily generalize the method to the case of general piecewise constant initial condition at the exit, just as for the entrance.

3.5 Solution procedure

In this section we summarize the solution procedure, concentrating on the discussion of finding the earliest time when the waves (characteristic lines or shocks or discontinuities) from the previous initial condition intersect with one another and hence the construction of the entropy solution must be restarted based on a new piecewise linear initial data.

Recall our assumption that the x-axis is divided into a number of elements, within each of which the initial density is given by a linear function $\rho(x, 0) = \alpha + \beta\, x$ that is completely contained in one of the regimes $\rho \le \rho_0$ or $\rho \ge \rho_0$. We consider several cases of wave

interactions separately below, and then take the smallest time from these cases, which will serve as the time to restart the solution procedure with a new piecewise linear initial data.

Once the smallest time of wave interactions is found, the density function is obtained at this time using the previous formulas as a new piecewise linear function, and the procedure is repeated, until the final desired time is reached.

For an element $\mathbf{e}$ in which the initial linear density profile is an increasing function, the natural break time, can be determined by the following formula (Whitham, 1974):

$$\tau_e = -\frac{1}{q''(\rho)\frac{\partial \rho}{\partial x}}$$

Notice that under our assumption (concave quadratic flux q and increasing linear density ρ) the denomination is a negative constant, hence τ_e is a positive constant. Indeed, if the element $\mathbf{e} = (x_l, x_r)$ and the initial condition density values at the element boundaries are $\rho_l = \rho(x_l^+, 0)$ and $\rho_r = \rho(x_r^-, 0)$, and assuming that the flux function in the element $\mathbf{e}$ is:

$$q(\rho) = a_0 + a_1\,\rho + a_2\,\rho^2$$

then

$$\tau_e = \begin{cases} \frac{x_r - x_l}{2a_2(\rho_l - \rho_r)} & \rho_r > \rho_l \\ \infty & \text{otherwise} \end{cases} \tag{55}$$

We now consider the situation that two adjacent nodes x_m and x_{m+1} correspond to a pair of adjacent characteristics and/or discontinuities which will intersect at time Δt. This is the most difficult case since no closed form formula exists for the intersecting time Δt. We will therefore resort to a nonlinear equation solver such as the Newton's method.

We denote $G_m(\Delta t) = \Delta x_m$. Likewise, the location of the trajectory from the node x_{m+1} at time Δt is $x_{m+1} + \Delta x_{m+1}$ and we denote $G_{m+1}(\Delta t) = \Delta x_{m+1}$. The displacements $G_m(\Delta t)$ and $G_{m+1}(\Delta t)$ are determined by (43) or (53) or (46). Therefore, we can define the function

$$S(\Delta t) = x_{m+1} - x_m + G_{m+1}(\Delta t) - G_m(\Delta t) \tag{56}$$

which measures the distance between the two shocks. Clearly, $S(0) = x_{m+1} - x_m > 0$, and we would like to find the root of $S(\Delta t)$, which corresponds to the time that the two shocks

intersect. As for each *fixed* Δt, $S(\Delta t)$ and $S'(\Delta t)$ can both be readily computed, we can easily set up a Newton iteration to solve for the root of $S(\Delta t)$ with $\Delta t = 0$ as the initial guess. We can follow the discussion in the appendix of Lu et al. (2006) to discuss the uniqueness of the solution to equation (56) before the natural break time, thereby facilitating the convergence of the Newton iteration process.

4 Numerical examples

In this section we provide three numerical examples to illustrate the explicit formulas for the entropy solutions obtained in the previous sections. The flow-density relationship is given by:

$$q(\rho) = \begin{cases} q_1(\rho) = -0.4\rho^2 + 100\rho, & 0 \le \rho \le 50 \\ q_2(\rho) = -0.02\rho^2 - 4\rho + 3850, & 50 < \rho \le 350. \end{cases}$$

see Figure 1. The units of flow and density are expressed in veh/h and veh/km, respectively. The discontinuity in the fundamental diagram occurs at $\rho = 50$ veh/km, and the flows on the immediate left and right of this continuity are $q = 4000$ veh/h and $q = 3600$ veh/h, respectively, with a capacity drop of 400 veh/h.

We also use the fifth order finite difference WENO scheme (Jiang and Shu, 1996; Lu et al., 2006; Zhang et al., 2003) to compute the solution and make a comparison. The purpose of this comparison is two fold: first to validate the computation of WENO schemes against the presumably exact entropy solutions obtained by the procedure in this paper; and second to demonstrate that high resolution numerical schemes such as the WENO schemes with adequate numerical viscosities do converge to the same entropy solutions that we obtain analytically in this paper for discontinuous fluxes. We remark that the choice of the viscosity coefficient in the Lax-Friedrichs building block of the WENO scheme must be chosen proportionally to $\frac{1}{\Delta x}$ when the initial condition crosses the discontinuity of the flux $\rho = \rho_0 = 50$, which is consistent with the analytical procedure adopted in this paper to derive entropy solutions, namely to use a sequence of approximate solutions with continuous fluxes with progressively sharper gradients and to take its limit to define the entropy solution corresponding

to the discontinuous flux.

The first and second numerical examples are generalized Riemann problems with the following initial and boundary conditions

$$\rho(x,0) = \begin{cases} \alpha_1 + \beta_1 x, & 0 \le x < 10 \\ \alpha_2 + \beta_2 x, & 10 \le x \le 20 \end{cases}, \qquad \rho(0,t) = \rho(0,0).$$

4.1 Example 1 (Shocks)

Example 1(a-1): $\alpha_1 = 20, \beta_1 = 0, \alpha_2 = 200, \beta_2 = 0$

We have

$$\frac{q_2(50) - q_1(20)}{50 - 20} > \frac{q_2(200) - q_2(50)}{200 - 50}.$$

Example 1(a-2): $\alpha_1 = 15, \beta_1 = 0.5, \alpha_2 = 200, \beta_2 = 1$

We have

$$\frac{q_2(50) - q_1(20)}{50 - 20} > \frac{q_2(210) - q_2(50)}{210 - 50}.$$

The solutions are shown in Figure 10.

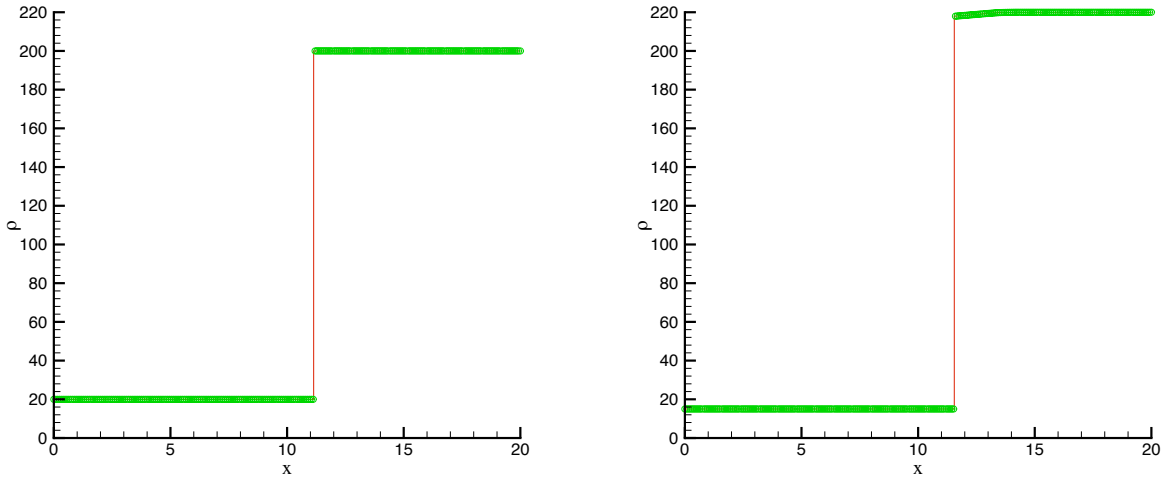

Figure 10: The exact entropy solution obtained by the procedure in Section 3 (solid line) and the numerical solution obtained by using WENO scheme with $N = 1000$ uniform grid points (circles) at the time t=30 min for Example 1 (a-1) and (a-2), respectively.

Example 1 (b-1): $\alpha_1 = 45, \beta_1 = 0, \alpha_2 = 80, \beta_2 = 0$

We have

$$\frac{q_2(50) - q_1(45)}{50 - 45} < \frac{q_2(80) - q_2(50)}{80 - 50}.$$

Example 1 (b-2): $\alpha_1 = 50, \beta_1 = -0.5, \alpha_2 = 80, \beta_2 = -1$

We have

$$\frac{q_2(50) - q_1(45)}{50 - 45} < \frac{q_2(70) - q_2(50)}{70 - 50}.$$

The solutions are shown in Figure 11.

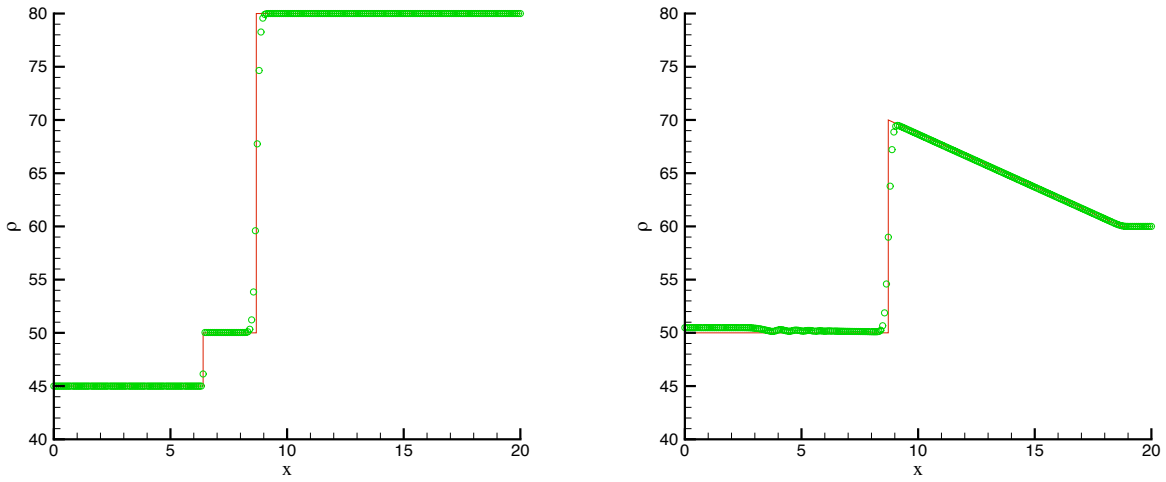

Figure 11: The exact entropy solution obtained by the procedure in Section 3 (solid line) and the numerical solution obtained by using WENO scheme with $N = 1000$ uniform grid points (circles) at the time t=12 min for Example 1 (b-1) and (b-2), respectively.

The exact solution of these problems can be worked out using the procedure in this paper, shown as solid lines in Figures 10 and 11, in comparison with the numerical solution obtained by the WENO scheme using $N = 1000$ uniform grid points, shown as circles. In both cases, we can see that the two results agree very well.

4.2 Example 2 (Rarefaction waves)

In this case $k_0 = -11.6569$ in (22)-(25).

Example 2 (a-1): $\alpha_1 = 300, \beta_1 = 0, \alpha_2 = 20, \beta_2 = 0$

$q_2'(300) < k_0$ and the solution is shown in Figure 12.

Example 2 (a-2): $\alpha_1 = 300, \beta_1 = 1, \alpha_2 = 30, \beta_2 = -1$

$q_2'(310) < k_0$ and the solution is also shown in Figure 12.

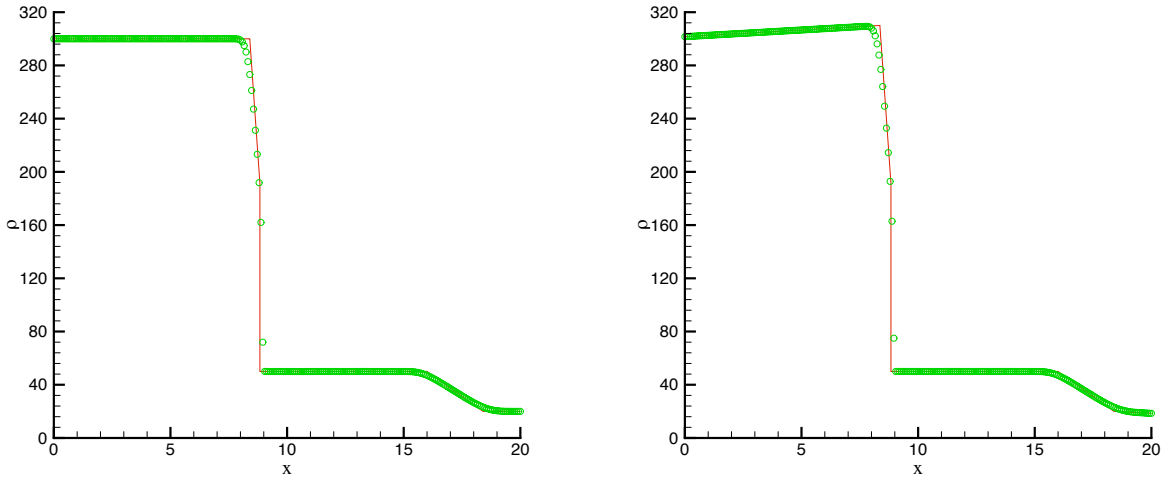

Figure 12: The exact entropy solution obtained by the procedure in Section 3 (solid line) and the numerical solution obtained by using WENO scheme with $N = 1000$ uniform grid points (circles) at the time t=6 min for Example 2 (a-1) and (a-2), respectively.

Example 2 (b-1): $\alpha_1 = 80, \beta_1 = 0, \alpha_2 = 20, \beta_2 = 0$

$q_2'(80) > k_0$ and the solution is shown in Figure 13.

Example 2 (b-2): $\alpha_1 = 80, \beta_1 = -1, \alpha_2 = 30, \beta_2 = -1$

$q_2'(70) > k_0$ and the solution is also shown in Figure 13.

The exact solution of these problems can be worked out using the procedure in this paper, shown as solid lines in Figures 12 and 13, in comparison with the numerical solution obtained by the WENO scheme using $N = 1000$ uniform grid points, shown as circles. Again, in both cases, we can see that the two results agree very well.

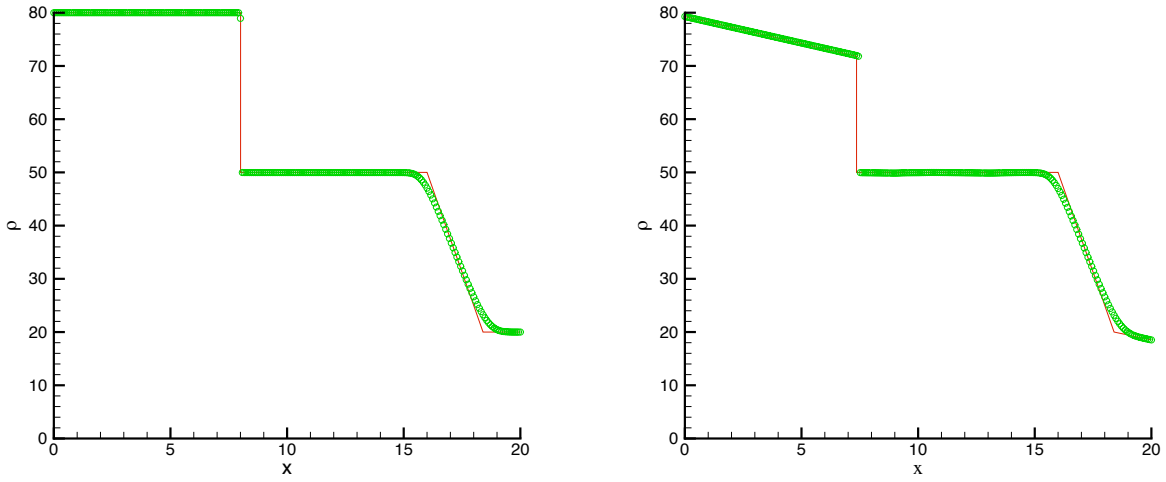

Figure 13: The exact entropy solution obtained by the procedure in Section 3 (solid line) and the numerical solution obtained by using WENO scheme with $N = 1000$ uniform grid points (circles) at the time t=6 min for Example 2 (b-1) and (b-2), respectively.

4.3 Example 3 (Wide moving jam)

Consider a long homogeneous freeway of length 30 km. We now assume the following initial density

$$\rho(x,0) = \begin{cases} 250, & 15 < x < 17 \\ \rho_d, & otherwise \end{cases}$$

which represents the traffic condition after an incident (recurrent or non-recurrent) at $x = 17$. The left-hand entrance of the highway is always kept at a density of ρ_d all time. We consider three cases: (a) $\rho_d = 50$, (b) $\rho_d = 45$, and (c) $\rho_d = 40$ veh/km, with entrance (demand) flows of 4000, 3690, and 3360 veh/h, respectively. The demand of the first two cases exceed the capacity of Flux II (3600 veh/h), whereas the demand of the third case is below this capacity. Figures 14-16 plot the exact entropy solution (solid line) and the numerical solution obtained by the fifth order WENO finite difference scheme with $N = 1000$ uniform grid points (circles) for all three cases. We can see that the two results agree very well.

From the figures, we can clearly see the formation of a wide moving jam with two very sharp shock fronts on both ends of the moving jam, which is a traffic phenomenon that is commonly observed on highways (Kerner and Rehborn, 1996), and was well studied using

the three-phase traffic theory (Kerner, 2004), cell transmission model (Lin and Lo, 2003), and traveling wave analysis (Jin and Zhang, 2003; Kerner and Konhauser, 1994; Zhang and Wong, 2006; Zhang et al., 2006). In Examples 3 (a) and 3 (b), when the demand from the left-hand highway entrance is higher than the capacity of the congested regime (Flux II in this example), the wide moving jam lasts for more than 30 minutes, whereas in Example 3 (c) when the demand is lower than this reduced capacity, the jam dissolves very quickly. It is interesting that the wide moving jam can also be formed using the first order LWR model, and does not require a linear flow-density relationship in the congested regime as discussed in Lin and Lo (2003).

We also show in Figure 17 the time-space diagrams and three-dimensional speed plots of these three cases to illustrate the results.

5 Conclusions

In this paper we consider the explicit construction of physically relevant entropy solutions of a class of conservation laws with discontinuous flux functions, which are piecewise quadratic and locally concave in each piece. We treat this problem as the limit of a sequence of approximate problems in which the fluxes are continuous functions but with progressively sharper gradients. We have presented explicit formulas for such entropy solutions for both the simple Riemann initial conditions and for piecewise linear initial conditions and piecewise constant boundary conditions. We demonstrate these explicitly constructed entropy solutions to representative traffic flow problems and compare them with numerical solutions obtained with high order WENO schemes.

6 Acknowledgements

The work of the second author was partially supported by a grant from the Research Grants Council of the Hong Kong Special Administrative Region, China (HKU7187/05E). The research of the third author was partially supported by the NSFC grant 10671190. The re-

search of the fourth author was partially supported by the NSFC grant 10671190 while this author was visiting the Department of Mathematics, University of Science and Technology of China, Hefei, Anhui 230026, P.R. China. Additional support was provided by ARO grant W911NF-04-1-0291 and NSF grant DMS-0510345.

References

[1] Ansorge, R., 1990. What does the entropy condition mean in traffic flow theory. Transportation Research Part B, 24 (2), 133-143.

[2] Bank, J.H., 1991a. Two-capacity phenomenon at freeway bottlenecks: a basis for ramp metering? Transportation Research Record, 1320, 83-90.

[3] Bank, J.H., 1991b. The two-capacity phenomenon: some theoretical issues. Transportation Research Record, 1320, 234-241.

[4] Cassidy, M.J., 1998. Bivariate relations in nearly stationary highway traffic. Transportation Research Part B, 32, 49-59.

[5] Cassidy, M.J. and Bertini, R.L., 1999. Some traffic features at freeway bottlenecks. Transportation Research Part B, 33, 25-42.

[6] Ceder, A., 1976. A deterministic traffic flow model for the two-regime approach. Transportation Research Record, 567, 16-32.

[7] Ceder, A., May, A.D., 1976. Further evaluation of single- and two-regime traffic flow models. Transportation Research Record, 567, 1-15

[8] Daganzo, C.F., 1995. A finite difference approximation of the kinematic wave model of traffic flow. Transportation Research Part B, 29 (4), 261-276.

[9] Drake, J.S., Schofer, J.L., May, A.D., 1967. A statistical analysis of speed density hypothesis. In L.C. Edie, R. Herman and R. Rothery (eds.) Proceedings of the Third Inter-

national Symposium on Theory of Traffic Flow, American Elsevier Publishing Company Inc., New York, USA.

[10] Edie, L.C., 1961. Car-following and steady-state theory for noncongested traffic. Operations Research, 9 (1), 66-76.

[11] Hall, F.L., 1987. An interpretation of speed-flow-concentration relationships using catastrophe theory. Transportation Research Part A, 21, 191-201.

[12] Hall, F.L. and Gunter, M.A., 1986. Further analysis of the flow-concentration relationship. Transportation Research Record, 1091, 1-9.

[13] Hall, F.L., Allen, B.L. and Gunter, M.A., 1986. Empirical analysis of freeway flow-density relationships. Transportation Research Part A, 20, 197-210.

[14] Jiang, G.S., Shu, C.W., 1996. Efficient implementation of weighted ENO schemes. Journal of Computational Physics, 126 (1), 202-228.

[15] Jin, W.L. and Zhang, H.M., 2003. The formation and structure of vehicle clusters in the Payne-Whitham traffic flow model. Transportation Research Part B, 37 (3), 207-223.

[16] Kerner, B.S., 2004. The Physics of Traffic: Empirical Freeway Pattern Features, Engineering Applications, and Theory, Springer, New York.

[17] Kerner, B.S., Konhauser, P., 1994. Structure and parameters of clusters in traffic flow. Physical Review E, 50 (1), 54-83.

[18] Kerner, B.S., Rehborn, H., 1996. Experimental features and characteristics of traffic jams. Physical Review E, 53 (2), R1297-R1300.

[19] Koshi, M., Iwasaki, M. and Ohkura, I., 1983. Some findings and an overview on vehicular flow characteristics. In V.F. Hurdle, R. Hauer and G.N. Stewart (eds) Proceedings of the 8th International Symposium on Transportation and Traffic Theory, University of Toronto Press, Toronto, Ontario, pp. 403-426.

[20] Lax, P., 1973. Hyperbolic Systems of Conservation Laws and the Mathematical Theory of Shock Waves, SIAM Regional Conference Series in Applied Mathematics, # 11, SIAM, Philadelphia.

[21] Lebacque, J.P., 1996. The Godunov scheme and what it means for first order traffic flow models. In J.B. Lesort (ed), Proceedings of the 13th International Symposium on Transportation and Traffic Theory, Elsevier Science Ltd, Lyon, France, pp. 647-677.

[22] LeVeque, R.J., 1992. Numerical Methods for Conservation Laws, Lecture in Mathematics, ETH Zurich, Birkhauser Verlag, Basel, Switzerland.

[23] Lighthill, M.J., Whitham, G.B., 1955. On kinetic wave II: a theory of traffic flow on crowded roads. Proceedings of the Royal Society of London, Series A, 229 (1178), 317-345.

[24] Lin, W.H. and Lo, H.K., 2003. A theoretical probe of a German experiment on stationary moving traffic jams. Transportation Research Part B, 37 (3), 251-261.

[25] Lu, Y., Wong, S.C., Zhang, M., Shu, C.-W., Chen, W., 2006. Explicit construction of entropy solutions for the LWR traffic flow model with a piecewise quadratic flow-density relationship and a comparison with the WENO scheme, submitted to Transportation Research Part B.

[26] May, A.D., and Keller, E.M., 1967. Non-integer car-following models. Highway Research Record, 199, 19-32.

[27] Michalopoulos, P.G., Beskos, D.E., Lin, J.K., 1984. Analysis of interrupted traffic flow by finite-difference methods. Transportation Research Part B, 18 (4-5), 409-421.

[28] Richards, P.I., 1956. Shock waves on the highway. Operations Research, 4 (1), 42-51.

[29] Velan, S., Florian, M., 2002. A note on the entropy solutions of the hydrodynamic model of traffic flow. Transportation Science, 36 (4), 435-446.

[30] Whitham, G.B., 1974. Linear and Nonlinear Waves, John Wiley & Sons, New York, USA.

[31] Wong, G.C.K., Wong, S.C., 2002a. A multi-class traffic flow model - an extension of LWR model with heterogeneous drivers. Transportation Research Part A, 36 (9), 827-841.

[32] Wong, S.C., Wong, G.C.K., 2002b. An analytical shock-fitting algorithm for LWR kinematic wave model embedded with linear speed-density relationship. Transportation Research Part B, 36 (8), 683-706.

[33] Zhang, M., Shu, C.W., Wong, G.C.K., Wong, S.C., 2003. A weighted essentially non-oscillatory numerical scheme for a multi-class Lighthill-Whitham-Richards traffic flow model. Journal of Computational Physics, 191 (2), 639-659.

[34] Zhang, P. and Wong, S.C., 2006. Essence of conservation forms in the traveling wave solutions of higher-order traffic flow models. Physical Review E, 74, 026109.

[35] Zhang, P., Wong, S.C. and Dai, S.Q., 2006. Characteristic parameters of a wide cluster in a higher-order traffic flow model. Chinese Physics Letters, 23, 516-519.

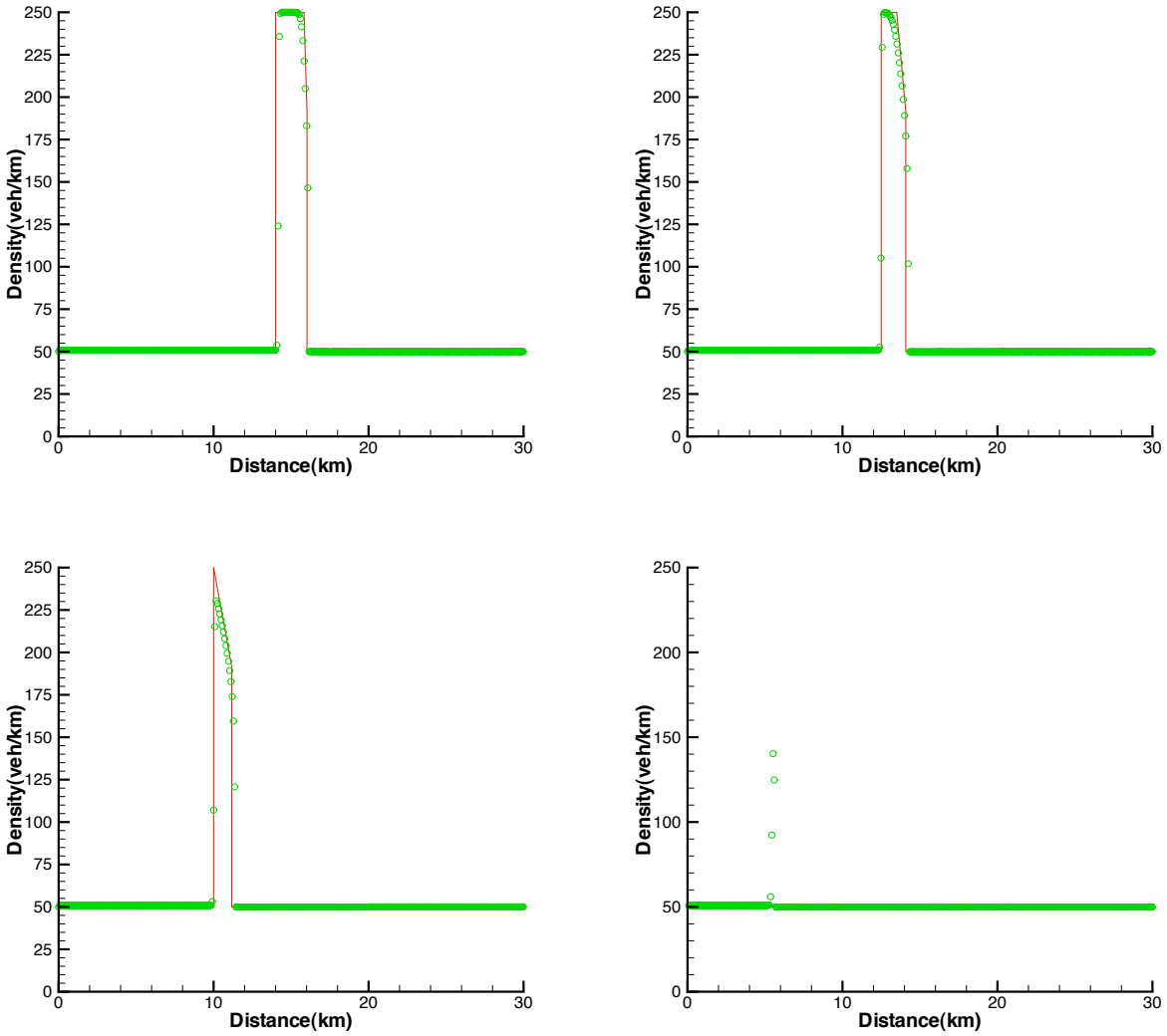

Figure 14: The exact entropy solution (solid line) and the numerical solution obtained by WENO scheme (circles) for Example 3 (a) $\rho_d = 50$. Top left: $t = 5$ min; top right: $t = 15$ min; bottom left: $t = 30$ min; bottom right: $t = 60$ min.

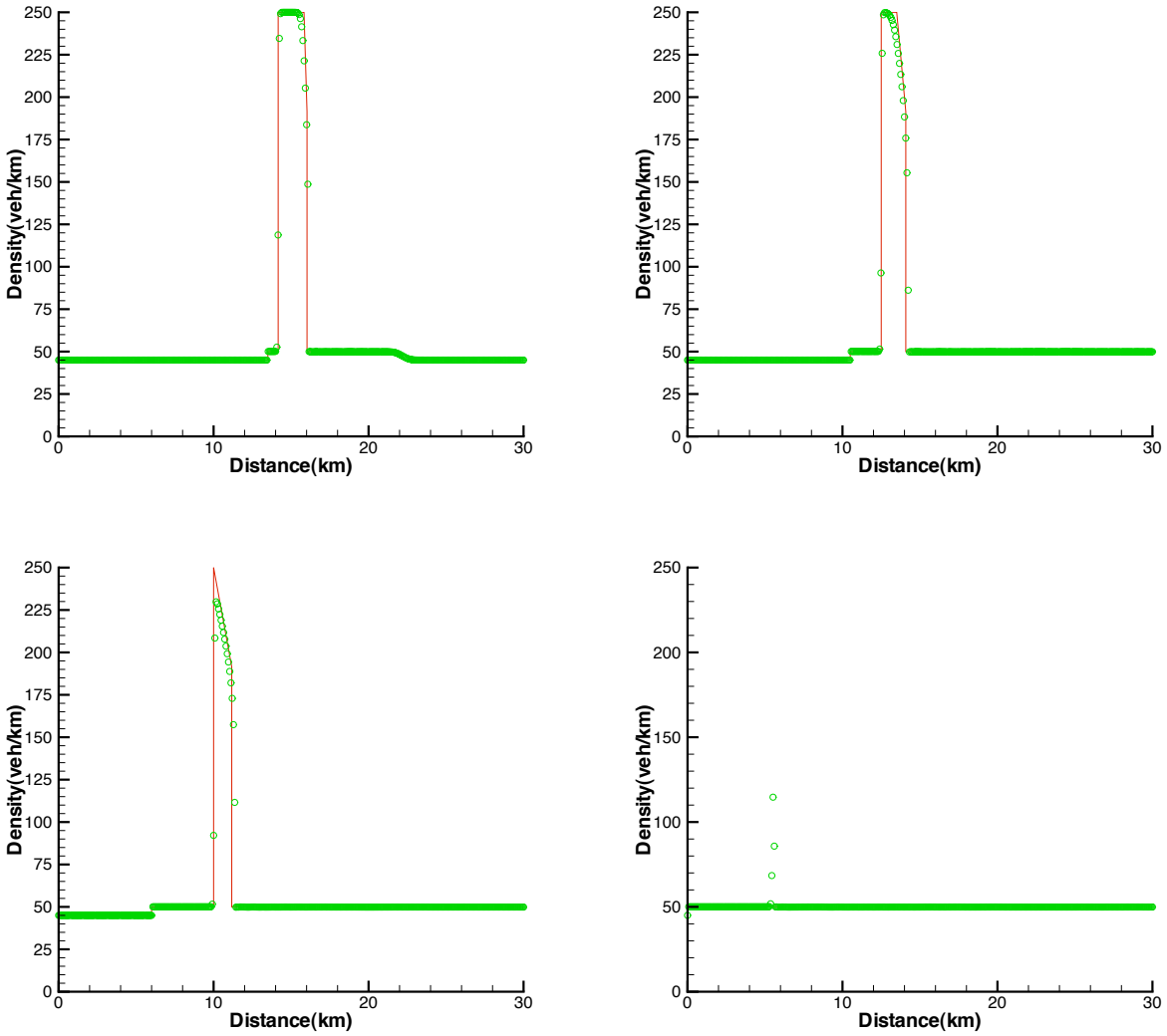

Figure 15: The exact entropy solution (solid line) and the numerical solution obtained by WENO scheme (circles) for Example 3 (b) $\rho_d = 45$. Top left: $t = 5$ min; top right: $t = 15$ min; bottom left: $t = 30$ min; bottom right: $t = 60$ min.

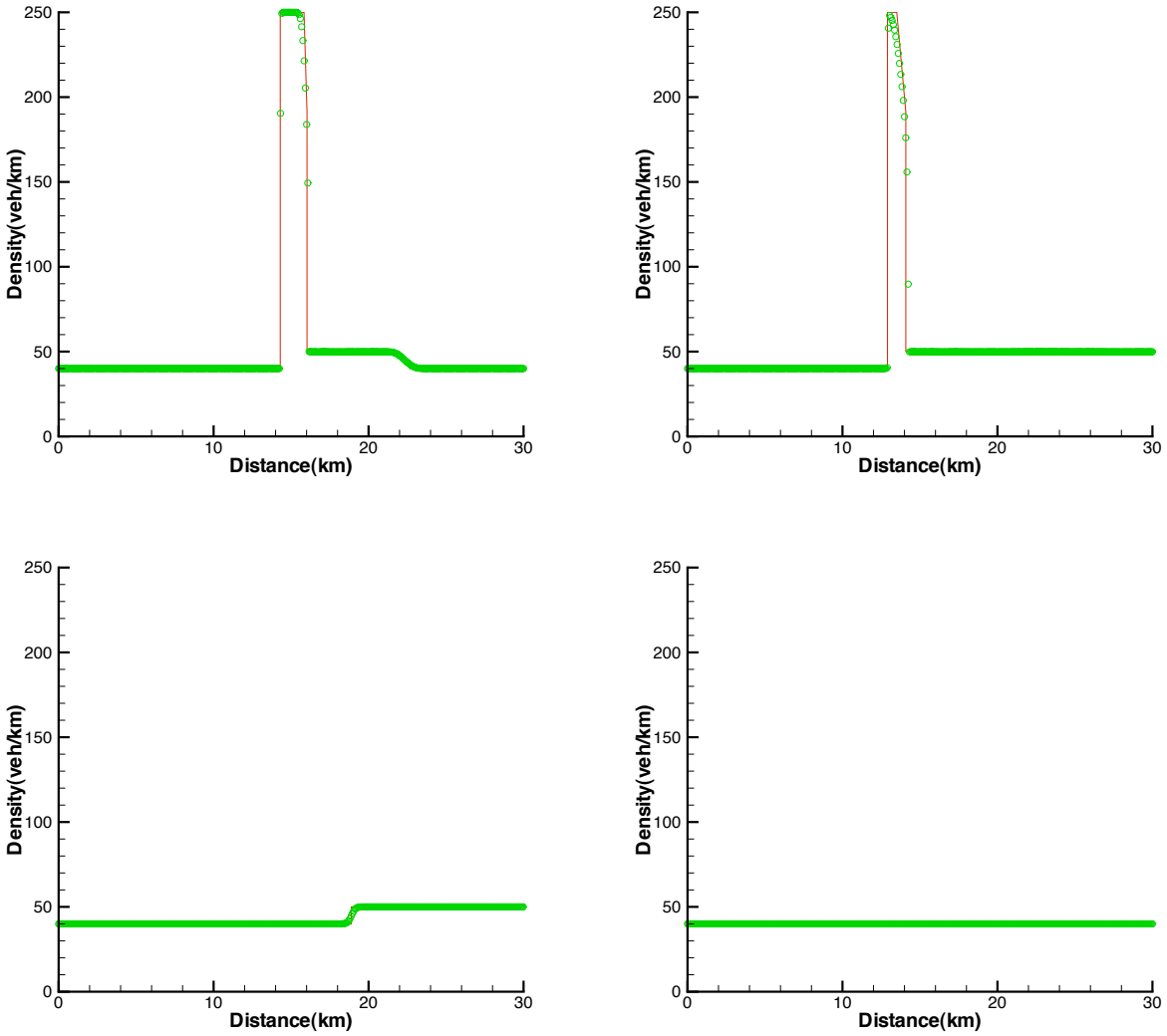

Figure 16: The exact entropy solution (solid line) and the numerical solution obtained by WENO scheme (circles) for Example 3 (c) $\rho_d = 40$. Top left: $t = 5$ min; top right: $t = 15$ min; bottom left: $t = 30$ min; bottom right: $t = 60$ min.

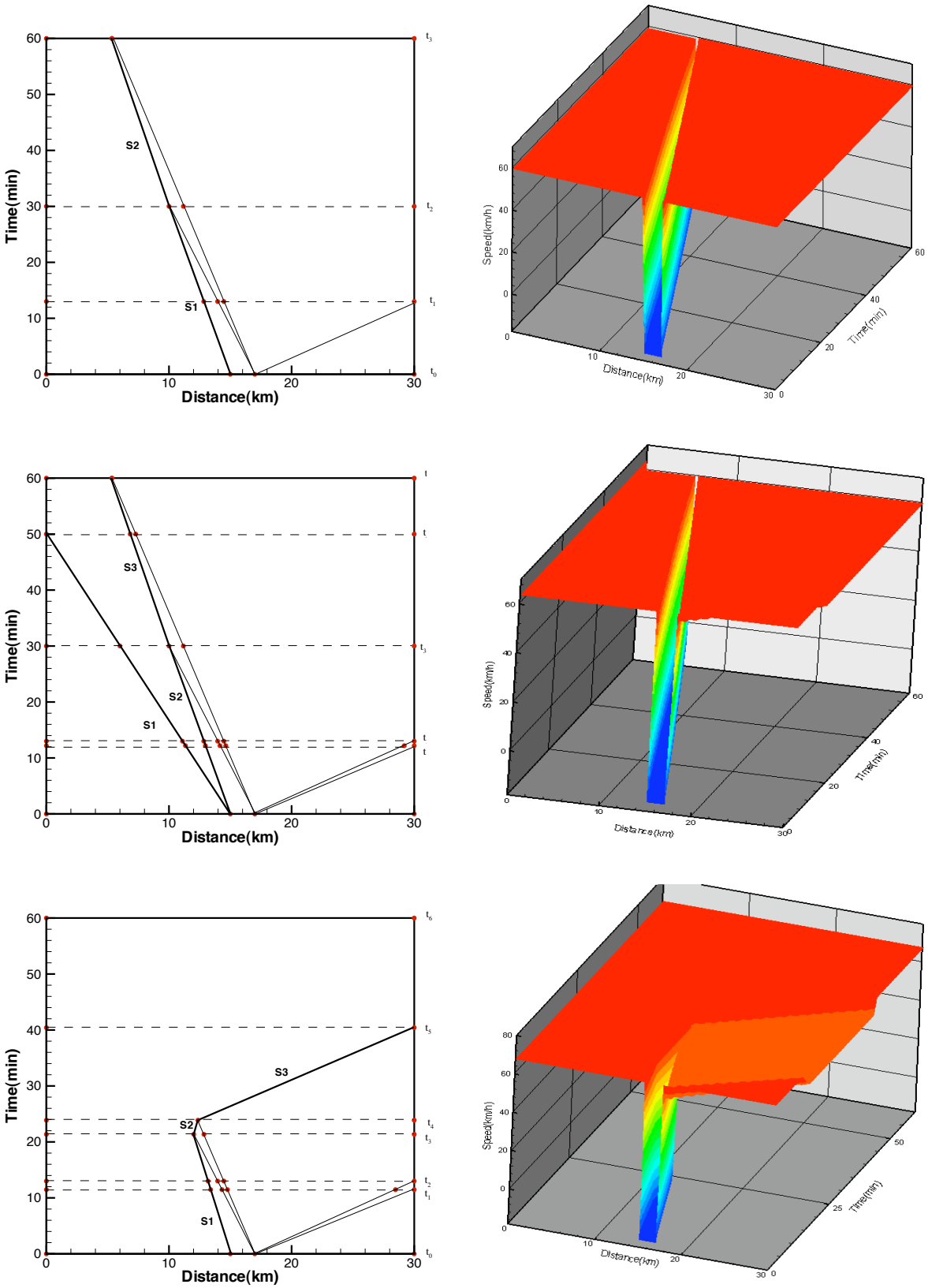

Figure 17: The exact entropy solutions for Example 3. Top: case (a); middle: case (b); bottom: case (c). Left: time-space diagram; right: 3D speed plot.